Estimating correlations and entanglement in the two-dimensional Heisenberg model in the strong-rung-coupling limit

Chandrima B. Pushpan, Harikrishnan K J, Prithvi Narayan, and Amit Kumar Pal
Department of Physics, Indian Institute of Technology Palakkad, Palakkad 678 623, India

We consider the isotropic Heisenberg model in a magnetic field in the strong-rung-coupling limit on a two-dimensional (2D) rectangular zig-zag lattice of arbitrary size, and determine the one-dimensional (1D) effective model representing the low-energy manifold of the 2D model up to second order in perturbation theory. We consider a number of Hermitian operators defined on the Hilbert space of the 2D model, and systematically work out their action on the low-energy manifold, which are operators on the Hilbert space of the 1D effective model. For a class of operators among them, we demonstrate that the expectation values computed in the low-energy manifold of the 2D model can be mimicked by the expectation values of the corresponding operators in the 1D effective model even beyond the perturbation regime of the system parameters. We further argue that quantitatively estimating partial trace-based measures of entanglement in the 2D model may be done in the same fashion only in the perturbation regime. Our results and approach are expected to be useful in investigating observables and entanglement in the 2D models with large system sizes due to the advantage of using the effective 1D model with a smaller Hilbert space as a proxy.

I. INTRODUCTION

The interface of quantum information theory [1] and *low-dimensional* interacting quantum spin systems [2], with small lattice dimension with each lattice site hosting a Hilbert space of a few levels, has grown into a rich area of interdisciplinary research [3–5] in the past two decades. On one hand, these interacting quantum spin models have been identified as the natural candidates for testing and implementing quantum information and computation protocols, such as quantum state transfer [6], measurement-based quantum computation [7], and topological quantum error corrections [8]. The motivation behind these studies has its origin in the natural occurrence of quantum states with rich quantum correlations belonging to both entanglement-separability [9] and quantum information theoretic paradigms [5], which, alongside being fundamentally important, can be used as resource in several quantum tasks [5,9]. On the other hand, these quantum correlations have provided a refreshing perspective of characterizing quantum many-body systems [3–5], along with the development of tools and techniques like projected entangled pair states [10] and multiscale entanglement renormalization ansatz [11]. Current experimental advances allowing implementation and manipulation of these quantum spin models as well as quantum protocols designed on these models using trapped ions [12], superconducting qubits [13], nuclear magnetic resonance [14], solid-state systems [15], and ultra-cold atoms [16] have also provided a major boost to these studies.

Among a plethora of low-dimensional quantum spin models, two-dimensional (2D) lattice models have always been specially challenging due to the faster growth of Hilbert space dimension with increasing number of spins in the system, compared to their one-dimensional (1D) counterparts. One

such model is the Heisenberg model [17] in a magnetic field on a rectangular lattice of NL sites, having respectively N and L lattice sites in the horizontal and vertical directions, where each lattice site hosts a spin-$1/2$ particle. A number of recent studies [18] have been carried out to understand the entanglement properties of the model. Particular attention has been drawn towards quasi-1D models [19] like quantum spin ladders [20,21] with the number of lattice sites in the horizontal direction being far greater than the same in the vertical direction ($N \gg L$). As natural extensions of the 1D models while going towards 2D, quantum spin ladders with $L = 2$ have been investigated from the perspective of quantum state transfer [22]. Moreover, entanglement [23] and fidelity [23] have been investigated in these ladder models from the perspective of characterization of phases. While most of these studies have concentrated on models with spin-$1/2$ particles, entanglement properties of quantum spin ladders with higher spin quantum numbers [24] have also been explored.

In the limit where the coupling strength $J_\perp$ along the vertical sublattices, referred to as the *rungs* of the ladder, are much larger compared to other spin-exchange interactions present in the system, the rung behaves like a single degree of freedom, and the model becomes effectively 1D. By further tuning magnetic field strength, for low values of L ($L = 2, 3$), Refs. [25–29] show that the isotropic Heisenberg quantum spin-$1/2$ ladders map to an 1D XXZ model [30,31] up to the first order in perturbation theory (see also [32]). This mapping has been used to study quantum phase transitions in the case of antiferromagentic spin-$1/2$ ladders with $L = 2$ [25–27,29] and 3 [28,29], using magnetization properties [25,29], and entanglement [27] of the mapped effective 1D XXZ model (see also [33] for the mapping in the case of a mixed-spin variant of quantum spin ladders with $L = 2$). While these case-by-case

studies have focused on obtaining the phase information of the isotropic Heisenberg Hamiltonian on the ladder-like lattices with low values of L using local observables and entanglement computed in the mapped 1D model, to the best of our knowledge, the possibility of computing the correlation functions and entanglement in the low-energy sector of the spin-1/2 Heisenberg model on the 2D lattice of *arbitrary size* using the effective 1D model as a proxy inside as well as outside the perturbation regime of the system-parameter space is yet to be explored. With this motivation, in this paper, we specifically focus on

(1) Determining the effective 1D model corresponding to the isotropic Heisenberg Hamiltonian on a zig-zag square lattice in the strong-rung-coupling limit for arbitrary size of the 2D lattice and

(2) Investigating whether the 1D effective model faithfully represent the spin correlation functions and entanglement computed using the states from the low-energy manifold of the 2D model even for parameter space points beyond the perturbation regime of the space of the system parameters.

Towards the first question, we determine the 1D effective model in a system size-independent fashion up to the first and the second order in perturbation theory, thereby bringing the specific models, studied so far in a case-by-case basis [25–29], under the same umbrella. We analytically derive the effective coupling constants of the 1D model as functions of the coupling constants in the original model for arbitrary size and for periodic boundary conditions on the 2D lattice in the vertical directions. We quantitatively specify the space of the system parameters, including the size L of a rung, in which the perturbation theory is valid so that the results from the 1D effective theory can be used. Using the energy gap, we also analyze the phase diagram of the 2D model. Further, for a number of operators defined on the Hilbert space of the 2D model, we systematically work out the operators they map to in the effective 1D model. Investigating the second question, we study the applicability of the 1D effective model in determining the energy gap and expectation values of operators in the 2D model irrespective of the chosen perturbation strength. More specifically, we show that both the energy gap, and the expectation values for a class of operators referred to as the *low-energy operators*, which does not take one out of the low-energy manifold (we define it precisely in Sec. III B), agree even beyond the perturbation regime of the system parameters. We further investigate such possibilities for entanglement in the 2D model, and argue that to quantitatively as well as qualitatively estimate entanglement in the low-lying states of the 2D model, one needs to choose the system parameters within the regime where perturbation theory is valid.

The rest of the paper is organized as follows. In Sec. II we discuss the 2D Heisenberg model (Sec. II A), the idea of the low-energy 1D effective Hamiltonian (Sec. II B), and its derivation for arbitrary size of the 2D lattice using the symmetry arguments and first- and second-order perturbation theory, where each rung is mapped to an effective qubit (Sec. II C). The phase information of the 2D isotropic Heisenberg model is explored using the 1D effective model in Sec. II E. Section III deals with the performance of the 1D effective theory in computing the energy gap, and expectation values of Hermitian operators defined on the 2D model
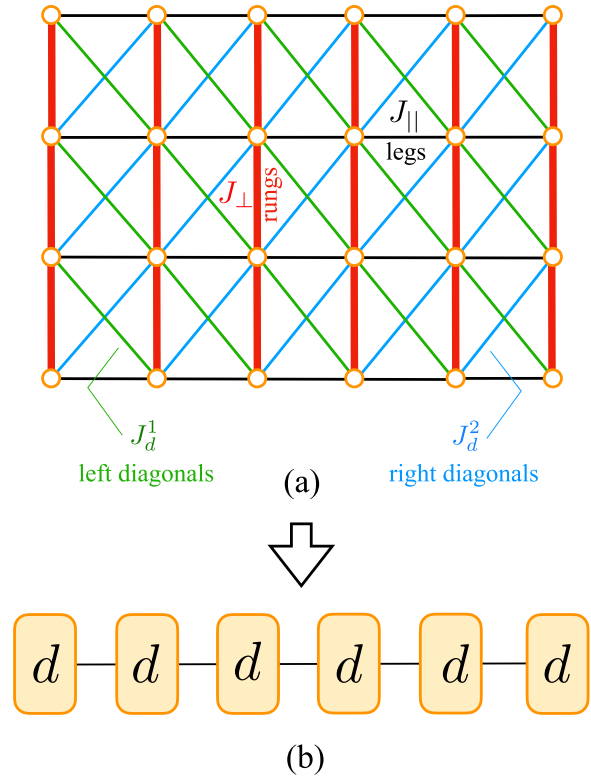

FIG. 1. (a) A 2D zig-zag lattice of six rungs and four legs holding 6×4 spin-$\frac{1}{2}$ particles. The spin-exchange interaction strength along the rungs and the legs are $J_\perp$ and $J_\parallel$, respectively, while the spins interact diagonally with the interaction strengths J_d^1 and J_d^2 along the left and the right diagonals respectively. The periodic boundary condition along the rungs, legs, and diagonals are represented by the dashed links to the edge spins of the lattice. Each spin in the lattice is subjected to a magnetic field of strength h in the z direction. (b) Using degenerate perturbation theory in the low-energy subspace in the strong-rung-coupling limit ($J_\perp \gg J_\parallel, J_d^1, J_d^2$), for specific points in the parameter space of $J_\perp$ and h, the model can be mapped to a effective 1D Hamiltonian [see Eq. (13)], where each lattice site hosts a d-dimensional Hilbert space corresponding to each rung of the system.

beyond the perturbation regime of the parameter space. It also discusses the computation of entanglement using partial trace-based approaches. Section IV contains the concluding remarks and outlook.

II. LOW-ENERGY EFFECTIVE HAMILTONIAN

In this section we introduce the isotropic Heisenberg model on the rectangular zig-zag lattice, and discuss mapping it to an effective 1D lattice model in the low-energy subspace, including the dependence of the validity of this mapping on the space of the system parameters, and the implication in extracting information about the phases of the 2D model.

A. Isotropic Heisenberg model on a 2D zig-zag lattice

Let us consider an $N \times L$ lattice with L (N) lattice sites along the vertical (horizontal) direction, each lattice site hosting a spin-$\frac{1}{2}$ particle [see Fig. 1(a)], such that a 2^{NL}-

dimensional Hilbert space $\mathcal{H}$ is associated to the system. We call the vertical (horizontal) lines in the lattice the *rungs* (*legs*), where N (L) represents the number of rungs (legs). While $N = L$ represents a zig-zag square lattice, $N \gg L$ represents a zig-zag *ladder* that is intermediate between the 1D and 2D lattices, and is therefore called a *quasi*-1D lattice model [21]. Isotropic Heisenberg interactions [30,31] are present between the spins along the legs, rungs, as well as the diagonals, and an external magnetic field applies to all spins along the z direction. The spin system is represented by the Hamiltonian [21]

$$H/J_\perp = H_R + H_I, \qquad (1)$$

with

$$H_R = \frac{1}{4} \sum_{i=1}^{N} \sum_{j=1}^{L} \vec{\sigma}_{i,j} \cdot \vec{\sigma}_{i,j+1} - \frac{h}{2J_\perp} \sum_{i=1}^{N} \sum_{j=1}^{L} \sigma_{i,j}^{z} - NE_g \qquad (2)$$

and

$$H_I = \frac{J_{||}}{4J_\perp} \sum_{i=1}^{N} \sum_{j=1}^{L} \vec{\sigma}_{i,j} \cdot \vec{\sigma}_{i+1,j} + \frac{J_d^1}{4J_\perp} \sum_{i=1}^{N} \sum_{j=1}^{L} \vec{\sigma}_{i,j+1} \cdot \vec{\sigma}_{i+1,j}$$

$$+ \frac{J_d^2}{4J_\perp} \sum_{i=1}^{N} \sum_{j=1}^{L} \vec{\sigma}_{i,j} \cdot \vec{\sigma}_{i+1,j+1}. \qquad (3)$$

Here $J_\perp$ ($J_{||}$) is the strength of the spin-exchange interactions along the rungs (along the legs), J_d^1 and J_d^2 are the diagonal interaction strengths, h is the strength of the magnetic field, $\vec{\sigma}_{i,j} \equiv \{\sigma_{i,j}^x, \sigma_{i,j}^y, \sigma_{i,j}^z\}$ are the Pauli operators on the lattice site denoted by the subscripts i, j, with i (j) being the rung (leg) index running from 1 to N (L), and E_g is a constant we will choose in Sec. II B. We use the computational basis $\{|0\rangle, |1\rangle\}$ to write the Pauli matrices, where $\sigma^z|0\rangle = |0\rangle$, $\sigma^z|1\rangle = -|1\rangle$, such that $|0\rangle \equiv |\uparrow\rangle$, and $|1\rangle \equiv |\downarrow\rangle$.

B. Effective Hamiltonian in low-energy subspace

We now discuss the construction of a low-energy effective 1D Hamiltonian (LEH) [32] corresponding to the spin models described in Sec. II A. We start with the limit $J_{||} = J_d^1 = J_d^2 = 0$, where the model consists of N noninteracting rungs, each of which corresponds to a 2^L-dimensional Hilbert space. The antiferromagnetic isotropic Heisenberg Hamiltonian of each rung is given by

$$H_{R_i} = \frac{1}{4} \sum_{j=1}^{L} \vec{\sigma}_{i,j} \cdot \vec{\sigma}_{i,j+1} - \frac{h}{2J_\perp} \sum_{j=1}^{L} \sigma_{i,j}^z - E_g, \qquad (4)$$

with $H_R = \sum_{i=1}^{N} H_{R_i}$. Let us assume that for a given value of h, the spectrum of H_{R_i} is given by $\{E_{k_i}^{(i)}, |\psi_{k_i}^{(i)}\rangle\}$, where $k_i \in \{0, 1, \ldots, 2^L - 1\} \, \forall i \in \{1, 2, \ldots, N\}$, such that

$$H_{R_i}|\psi_{k_i}^{(i)}\rangle = E_{k_i}^{(i)}|\psi_{k_i}^{(i)}\rangle, \qquad (5)$$

with $k_i = 0$ representing the ground state. A d-fold degeneracy in the ground states can be imposed via tuning h to specific values, which we denote by h', where typically $h' \sim J_\perp$ (see the Appendix for details in the case of $d = 2$). At this point, we choose E_g such that ground state energy of H_R with $h = h'$

vanishes. For a fixed L, there may be multiple values of h' resulting in different degeneracies d of the ground states. For each h', we relabel the states $\{|\psi_{k_i}^{(i)}\rangle\}$ such that

$$E_{k_i}^{(i)} = 0 \, \forall \, k_i = 0, 1, 2, \ldots, d-1, \qquad (6)$$

$$E_{k_i}^{(i)} > 0 \, \forall \, k_i = d, d+2, \ldots, 2^L - 1, \qquad (7)$$

and denote the d-fold degenerate ground states by $\{|\psi_0^{(i)}\rangle, \ldots, |\psi_{d-1}^{(i)}\rangle\}$. For each h', the ground-state manifold $\{|\Psi_l\rangle\}$ of H_R is d^N-fold degenerate, constituting the ground state subspace $\mathcal{S} \subset \mathcal{H}$ of the system of N noninteracting rungs, with $|\Psi_l\rangle$ having the form

$$|\Psi_l\rangle = \bigotimes_{i=1}^{N} |\psi_{k_i}^{(i)}\rangle. \qquad (8)$$

Here $k_i = 0, 1, \ldots, d-1$, and $l = 0, 1, 2, \ldots, d^N - 1$ labels the ground state manifold (note that l can be identified as the decimal equivalent of the string $k_1 k_2 k_3 \cdots k_N$ in base d). We will find it useful to split the Hilbert space into two subspaces, one is the subspace spanned by $|\Psi_l\rangle$ (which we will term the *low-energy sector*) and the other (which we will term the *high-energy sector*) orthogonal to this space. We can also define a projector onto the low-energy sector as

$$P_g = \sum_l |\Psi_l\rangle\langle\Psi_l|, \qquad (9)$$

and the projector on the high-energy sector is $P_e \equiv I - P_g$.

Let us now rewrite the system Hamiltonian H [Eq. (1)] as

$$\frac{1}{J_\perp} H = H_0 + \frac{1}{J_\perp} H', \qquad (10)$$

where

$$H_0 = \frac{1}{4} \sum_{i=1}^{N} \sum_{j=1}^{L} \vec{\sigma}_{i,j} \cdot \vec{\sigma}_{i,j+1} - \frac{h'}{2J_\perp} \sum_{i=1}^{N} \sum_{j=1}^{L} \sigma_{i,j}^z - NE_g, \qquad (11)$$

which is H_R at $h = h'$, and

$$H' = \frac{J_{||}}{4} \sum_{i=1}^{N} \sum_{j=1}^{L} \vec{\sigma}_{i,j} \cdot \vec{\sigma}_{i+1,j} + \frac{J_d^1}{4} \sum_{i=1}^{N} \sum_{j=1}^{L} \vec{\sigma}_{i,j+1} \cdot \vec{\sigma}_{i+1,j}$$

$$+ \frac{J_d^2}{4} \sum_{i=1}^{N} \sum_{j=1}^{L} \vec{\sigma}_{i,j} \cdot \vec{\sigma}_{i+1,j+1} - \frac{\Delta h}{2} \sum_{i=1}^{N} \sum_{j=1}^{L} \sigma_{i,j}^z, \qquad (12)$$

with $\Delta h = h - h'$. Clearly, ground states of H_0 have a d^N-fold degeneracy [see Eq. (8)], which is lifted by the perturbation H'. For $\Delta h, J_{||}, J_d^{1,2} \ll J_\perp$, this leads to an effective Hamiltonian operating in the low-energy subspace $\mathcal{S}$, where energy eigenvalues of the nth order ($n = 1, 2, \ldots$) effective Hamiltonian in $\mathcal{S}$ provides the nth-order energy corrections to the unperturbed states of low energy. In this paper, we focus only on the first- ($n = 1$) and the second-order ($n = 2$) effective Hamiltonians, which can be obtained as

$$\tilde{H}^{(1)} = \sum_{l,l'=0}^{d^N-1} \langle\Psi_l|H'|\Psi_{l'}\rangle |\Psi_l\rangle\langle\Psi_{l'}|, \qquad (13)$$

$$\tilde{H}^{(2)} = \sum_{l,l'=0}^{d^N-1} \sum_m \frac{1}{E_m} \langle\Psi_l|H'|\xi_m\rangle\langle\xi_m|H'|\Psi_{l'}\rangle |\Psi_l\rangle\langle\Psi_{l'}|, \qquad (14)$$

where $\{|\xi_m\rangle\}$ are states from the high-energy sector of H_0 such that $H_0|\xi_m\rangle = E_m|\xi_m\rangle$, which are connected to $\{|\Psi_l\rangle\}$ by H'. Note here that both the first- and the second-order effective Hamiltonians [Eqs. (13) and (14)] are operators on the Hilbert space of a system of one lattice dimension with N sites, where each lattice site has d degrees of freedom.

C. Special cases: $d = 2$

In this paper we focus on a subset of cases with $d = 2$ by choosing h' appropriately (see the Appendix for details). The effective degrees of freedom in this case is like a spin-1/2 system. The effective Hamiltonian will be built out of operators acting on this low-energy spin-1/2 degree of freedom. Towards this, let us first define

$$\tau_i^x = |\psi_0^{(i)}\rangle\langle\psi_1^{(i)}| + |\psi_1^{(i)}\rangle\langle\psi_0^{(i)}|, \tag{15}$$

$$\tau_i^y = -i\big[|\psi_0^{(i)}\rangle\langle\psi_1^{(i)}| - |\psi_1^{(i)}\rangle\langle\psi_0^{(i)}|\big], \tag{16}$$

$$\tau_i^z = |\psi_0^{(i)}\rangle\langle\psi_0^{(i)}| - |\psi_1^{(i)}\rangle\langle\psi_1^{(i)}| \tag{17}$$

as the effective Pauli-x, y, and z operators on the rung subspace spanned by $|\psi_{0,1}^{(i)}\rangle$. Next, we work out the symmetries of the system which will constrain the structure of the effective Hamiltonians, and the detailed structure of the effective Hamiltonians can be subsequently worked out. We denote the doubly degenerate ground states of H_{R_i} at $h = h'$ by $|\psi_0^{(i)}\rangle$ and $|\psi_1^{(i)}\rangle$. Since $[Z_i, H_{R_i}] = 0$, with $Z_i = \sum_{j=1}^L \sigma_{i,j}^z$ defined on the rung i,

$$Z_i|\psi_k^{(i)}\rangle = m_k|\psi_k^{(i)}\rangle, \tag{18}$$

$k = 0, 1$, where m_k are the eigenvalues of Z_i corresponding to the eigenvectors $|\psi_k^{(i)}\rangle$. Note here that Z_i is the generator of the z rotation on the Hilbert space of the ith rung with

$$J_i^z = a + bZ_i, \tag{19}$$

where a and b are real constants that can be chosen according to convenience [see Eq. (18) for the definition of Z_i]. If $m_0 \neq m_1$, we choose $a = (m_1 + m_0)/(m_1 - m_0)$ and $b = 2/(m_0 - m_1)$ such that

$$J_i^z|\psi_0^{(i)}\rangle = |\psi_0^{(i)}\rangle, \quad J_i^z|\psi_1^{(i)}\rangle = -|\psi_1^{(i)}\rangle. \tag{20}$$

Therefore, the action of J_i^z on the rung subspace spanned by $|\psi_{0(1)}^{(i)}\rangle$ is similar to that of an *effective* Pauli-z operator (note that the assumption $m_0 \neq m_1$ is crucial for the J_i^zs to mimic the action of Pauli-z operators), which is given in Eq. (17). Further, consider the operator

$$\mathcal{Z} = \sum_{i=1}^N J_i^z, \tag{21}$$

where $\mathcal{Z}$ is a symmetry of the original system-Hamiltonian H,

$$[\mathcal{Z}, H_0] = [\mathcal{Z}, H'] = 0, \tag{22}$$

and $\mathcal{Z}$ and $\eta^z = \sum_{i=1}^N \tau_i^z$ are equivalent.

We now argue that the effective Hamiltonian preserves the rotational symmetry in z direction to the second order in

perturbation theory in $J_\perp^{-1}$. More precisely, we write

$$\tilde{H} = \sum_{n=0}^2 J_\perp^{-n} \tilde{H}^{(n)} + \cdots, \tag{23}$$

and note that general formalism of perturbation theory provides [32]

$$\tilde{H} = P_g H_0 P_g + \frac{1}{J_\perp} P_g H' P_g$$
$$+ \frac{1}{J_\perp^2} P_g H' P_e H_0^{-1} P_e H' P_g + \cdots. \tag{24}$$

Since the only operators on the right-hand side are H' and P_g [Eq. (9)], and since $[H', \mathcal{Z}] = 0$ and $[P_g, \mathcal{Z}] = 0$—the former is simply the consequence of rotational symmetry of the 2D system [Eq. (1)] and the latter can be seen directly from the fact that $|\Psi_l\rangle$ is an eigenvector of the Hermitian operator $\mathcal{Z}$—it is straightforward to see that $[\tilde{H}, \mathcal{Z}] = 0$, and consequently $[\tilde{H}, \eta^z] = 0$.

1. Effective Hamiltonian up to second order

Since the first-order effective Hamiltonian is guaranteed to be at most nearest-neighbor in the effective spins, the most general form of z-rotationally invariant $\tilde{H}$ [$= J_\perp^{-1}\tilde{H}^{(1)}$; see Eq. (23)] is a nearest-neighbor XXZ model [30] in a magnetic field, given by

$$\tilde{H} = \tilde{J}_{xy}^{(1)}\left[\sum_{i=1}^N \big(\tau_i^x\tau_{i+1}^x + \tau_i^y\tau_{i+1}^y + \tilde{\delta}^{(1)}\tau_i^z\tau_{i+1}^z\big) + \tilde{g}^{(1)}\sum_{i=1}^N \tau_i^z\right], \tag{25}$$

with the dimensionless parameters $\tilde{J}_{xy}^{(1)}$, $\tilde{g}^{(1)}$, and $\tilde{\delta}^{(1)}$ given by (see Sec. 1 in the Appendix)

$$\tilde{J}_{xy}^{(1)} = \frac{1}{4J_\perp}\big(J_{||} - J_d^{sum}\big),$$

$$\tilde{g}^{(1)} = \frac{\tilde{h}^{(1)}}{\tilde{J}_{xy}^{(1)}} = 2\left[\frac{(L-1)\big(J_{||} + J_d^{sum}\big) - L\Delta h}{L\big(J_{||} - J_d^{sum}\big)}\right],$$

$$\tilde{\delta}^{(1)} = \frac{\tilde{J}_{zz}^{(1)}}{\tilde{J}_{xy}^{(1)}} = \frac{J_{||} + J_d^{sum}}{L\big(J_{||} - J_d^{sum}\big)}, \tag{26}$$

where $\tilde{J}_{xy}^{(1)} \neq 0$ (i.e., $J_{||} \neq J_d^{sum}$), and we have defined $J_d^{sum} = J_d^1 + J_d^2$, assumed periodic boundary conditions (PBC) along both rungs and legs, i.e., $\vec{\sigma}_{N+1,j} \equiv \vec{\sigma}_{1,j}$ and $\vec{\sigma}_{i,L+1} \equiv \vec{\sigma}_{i,1}$, and have considered $L(> 2)$ to be even in order to ensure $d = 2$. The periodic and open boundary conditions along the rung are equivalent for $L = 2$, a case which we work out separately, and get (see Sec. 1 in the Appendix)

$$\tilde{J}_{xy}^{(1)} = \frac{1}{8J_\perp}\big(2J_{||} - J_d^{sum}\big),$$

$$\tilde{g}^{(1)} = \frac{\tilde{h}^{(1)}}{\tilde{J}_{xy}^{(1)}} = \frac{2J_{||} + J_d^{sum} - 4\Delta h}{2J_{||} - J_d^{sum}},$$

$$\tilde{\delta}^{(1)} = \frac{\tilde{J}_{zz}^{(1)}}{\tilde{J}_{xy}^{(1)}} = \frac{2J_{||} + J_d^{sum}}{2\big(2J_{||} - J_d^{sum}\big)}, \tag{27}$$

where $\tilde{J}_{xy}^{(1)} \neq 0$ (i.e., $2J_{||} \neq J_d^{\text{sum}}$). In this picture, we relabel $|\psi_{0,1}^{(i)}\rangle$ as

$$|\mathbf{0}_i\rangle = |\psi_0^{(i)}\rangle, |\mathbf{1}_i\rangle = |\psi_1^{(i)}\rangle, \tag{28}$$

where $\{|\mathbf{0}_i\rangle, |\mathbf{1}_i\rangle\}$ form the τ^z eigenbasis of the spin-1/2 particle at the ith site of the 1D lattice of size N, representing an effective computational basis. Eigenstates of the 1D model [given in (25)], $|\tilde{\Phi}_l\rangle$, can be written in terms of the $\{|\mathbf{0}_i\rangle, |\mathbf{1}_i\rangle\}$ basis of the effective spins in the system.

The second-order effective Hamiltonian $\tilde{H} = J_\perp^{-1}\tilde{H}^{(1)} + J_\perp^{-2}\tilde{H}^{(2)}$ [see Eq. (23)] can be at most next-nearest-neighbor in the effective spins. For even L (≥ 4), and PBC along both rungs and legs, we derive the effective Hamiltonian, up to the second order in perturbation theory, as (see Sec. 2 in the Appendix for the derivation)

$$\tilde{H} = \tilde{J}_{xy}^{(2)}\Bigg[\sum_{i=1}^{N} \left(\tau_i^x \tau_{i+1}^x + \tau_i^y \tau_{i+1}^y + \tilde{\delta}^{(2)} \tau_i^z \tau_{i+1}^z \right) + \tilde{g}^{(2)} \sum_{i=1}^{N} \tau_i^z$$
$$+ \tilde{\gamma}^{(2)} \sum_{i=1}^{N} \left(\tau_{i-1}^x \tau_{i+1}^x + \tau_{i-1}^y \tau_{i+1}^y \right)\left(I_i - \tau_i^z \right) \Bigg], \tag{29}$$

where $\tilde{J}_{xy}^{(2)} \neq 0$, and

$$\tilde{J}_{xy}^{(2)} = \frac{1}{4J_\perp}\left(J_{||} - J_d^{\text{sum}} \right),$$

$$\tilde{\delta}^{(2)} = \tilde{\delta}^{(1)} + \frac{GJ_\perp}{J_{||} - J_d^{\text{sum}}} + \frac{F}{2}\left(\frac{J_{||} - J_d^{\text{sum}}}{J_\perp} \right),$$

$$\tilde{\gamma}^{(2)} = \frac{F}{4}\left(\frac{J_{||} - J_d^{\text{sum}}}{J_\perp} \right),$$

$$\tilde{g}^{(2)} = \tilde{g}^{(1)} - \frac{2GJ_\perp}{J_{||} - J_d^{\text{sum}}} - F\left(\frac{J_{||} - J_d^{\text{sum}}}{J_\perp} \right). \tag{30}$$

To keep the main text uncluttered, details on the calculation of the factors F and G and their explicit forms are given in Sec. 2 in the Appendix. The case of $L = 2$, similar to the first-order calculation, has to be worked out separately, and we have included it in Sec. 2 in the Appendix. It is noteworthy that for $J_d^{\text{sum}} = 0$ (which is possible, for example, in the case of the absence of the diagonal interactions, i.e., $J_d^1 = J_d^2 = 0$), Eqs. (29) and (30) also describe the $L = 2$ case.

We point out here that the exact forms of the effective system parameters ($\tilde{J}_{xy}^{(1)}$, $\tilde{g}^{(1)}$, $\tilde{\delta}^{(1)}$) in the case of the first-order effective theory, or ($\tilde{J}_{xy}^{(2)}$, $\tilde{g}^{(2)}$, $\tilde{\delta}^{(2)}$, $\tilde{\gamma}^{(2)}$) in the case of second-order effective theory as functions of the system parameters $J_{||}/J_\perp$, $J_d^{1,2}/J_\perp$, and $\Delta h/J_\perp$ of the 2D Hamiltonian depend on the forms of the doubly degenerate ground states $|\psi_{0,1}^{(i)}\rangle$, and subsequently on the specific point $h = h'$ where the perturbation calculation is carried out. For example, an open boundary condition (OBC) along the legs ($\vec{\sigma}_{N+1,j} \not\equiv \vec{\sigma}_{1,j}$) in the above calculation results in corrections in the effective magnetic field strengths on the boundary sites 1 and N on the effective 1D lattice, shown explicitly in the case of the first-order effective Hamiltonian in Sec. 1 in the Appendix. One can also consider OBC along the rungs ($\vec{\sigma}_{i,L+1} \not\equiv \vec{\sigma}_{i,1}$), for which determining the value of h' and the forms of $|\psi_{0,1}^{(i)}\rangle$ is difficult for arbitrary L. See Sec. 3 in the Appendix for the
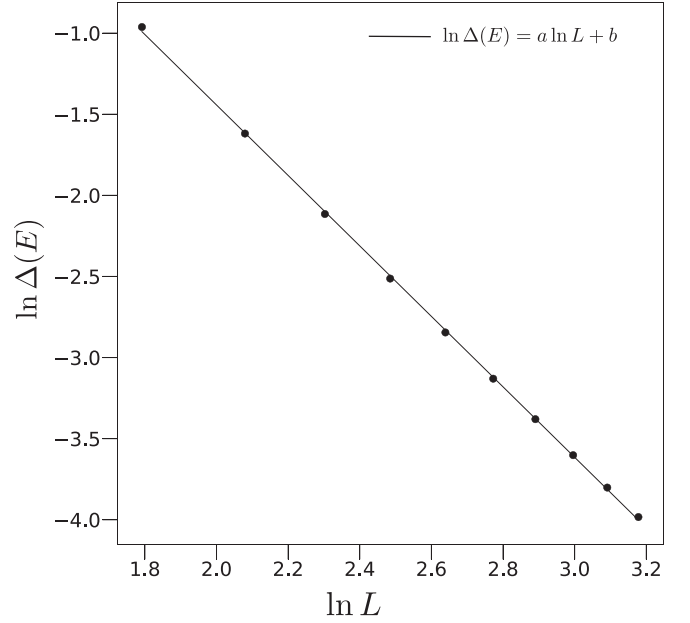

FIG. 2. Variation of the energy gap $\Delta E(L)$ between the doubly degenerate ground state and the excited state manifold of a rung of L spins with $J_\perp = 1$, where L is large. The data fit the equation $\ln \Delta E(L) = a \ln L + b$ with the fitting constants are $a = -2.172$ and $b = 2.901$, where we have considered only even values of L in the range $6 \leqslant L \leqslant 24$. All quantities plotted are dimensionless.

corresponding details on the first-order effective Hamiltonian. We would like to mention further that one can also extend the study towards higher orders in perturbation theory, and the details of the 1D effective model would accordingly change with an introduction of longer than next-to next-nearest-neighbor interactions, and beyond three-site spin interactions. While working out these details is possible (but somewhat tedious), we refrain from going beyond the second order in perturbation theory in this paper.

D. Validity of the perturbation theory

We now ask whether this treatment applies to a 2D Hamiltonian H with a fixed large value of $J_\perp$ on a lattice with arbitrary values of N and L. With increasing L, the energy gap $\Delta E(L)$ between the doubly degenerate ground state manifold and the excited state manifold decreases polynomially with L as $\sim L^{-2.172}$ for large L [see Fig. 2 for a typical variation of $\Delta E(L)$ with L for $J_\perp = 1$]. Therefore, in order to apply perturbation theory for the 2D model with different large values of L and to ensure negligible contribution from the terms of the Hamiltonian connecting the degenerate ground state manifold with the excited state manifold, one needs to be in the following regime of parameter space:

$$|J_{||}/J_\perp|, |\Delta h/J_\perp|, |J_d^{1,2}/J_\perp| \ll L^{-2.172}. \tag{31}$$

Unless otherwise stated, for all demonstrations in the rest of the paper, we fix $J_\perp = 1$. Further, for a fixed value of L, we assume antiferromagnetic interactions, and vary the values of these interaction strengths within the range

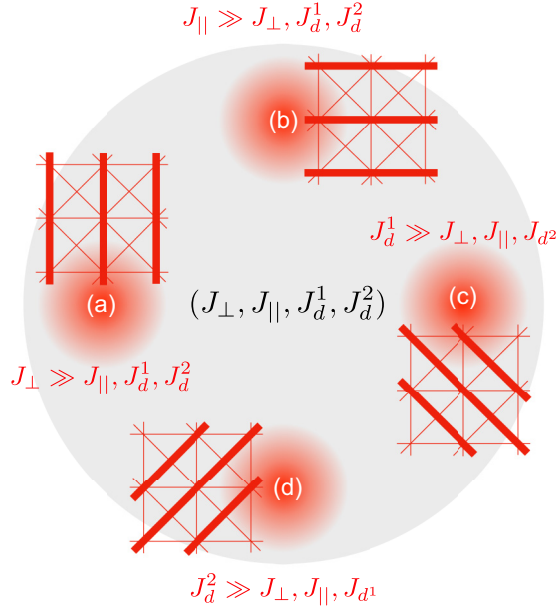$$0 \leqslant J_{||}/J_\perp, |\Delta h/J_\perp|, J_d^{1,2}/J_\perp \leqslant \Delta E(L)/10. \tag{32}$$

FIG. 3. Schematic representation of the subspaces denoted by (a) $J_\perp \gg J_{||}, J_d^1, J_d^2$, (b) $J_{||} \gg J_\perp, J_d^1, J_d^2$, (c) $J_d^1 \gg J_\perp, J_{||}, J_d^2$, and (d) $J_d^2 \gg J_\perp, J_{||}, J_d^1$ in the space of the parameters $J_\perp, J_{||}, J_d^1,$ and J_d^2. The thick lines in the lattices represent the strong couplings. While this paper deals with only the subspace (a), the 1D effective model in each of these subspaces can be worked out following the same methodology discussed in Sec. II.

Also, we consider the interaction strengths to be outside the perturbation region if

$$\Delta E(L)/10 < J_{||}/J_\perp, |\Delta h/J_\perp|, J_d^{1,2}/J_\perp \leqslant \Delta E(L)/2. \quad (33)$$

We would like to reemphasize here that while our results for 1D effective Hamiltonian in perturbation theory is valid for all L; see, for instance, the L dependence of effective couplings in Eq. (A14), the regime of validity of perturbation theory in the space of couplings $(J_\perp, J_{||}, J_d^{1,2}, h)$ gets squeezed at large L as per Eq. (32). Note further that the formalism discussed through Sec. II can be applied to the strong leg, left-diagonal, and right-diagonal limits also. This provides a large subspace in the parameter space of the coupling constants of the 2D model where the 1D effective theory works. See Fig. 3 for an illustration.

E. Phase diagrams

We now discuss the phase diagram of the 2D model, probed via the first- and second-order effective Hamiltonians given respectively in Eqs. (25) and (29).

1. Phase diagram up to the first order

We now focus on the first-order effective Hamiltonian [Eq. (25)] and note that the physics of the 1D model itself remains invariant with a change in the value of $\tilde{J}_{xy}^{(1)}$. Fixing $\tilde{J}_{xy}^{(1)} = 1$, and using $\tilde{g}^{(1)}$ and $\tilde{\delta}^{(1)}$, the phase diagram corresponding to $\tilde{H}$ [Eq. (25)] is given by Fig. 4(a). Solving for $J_{||}/J_\perp$, $J_d^{sum}/J_\perp$, and $\Delta h/J_\perp$ in terms of $\tilde{g}^{(1)}$, $\tilde{\delta}^{(1)}$, and $\tilde{J}_{xy}^{(1)}$ for $L > 2$, one can write

$$\frac{J_{||}}{J_\perp} = 2\tilde{J}_{xy}^{(1)}(L\tilde{\delta}^{(1)} + 1),$$

$$\frac{J_d^{sum}}{J_\perp} = 2\tilde{J}_{xy}^{(1)}(L\tilde{\delta}^{(1)} - 1),$$

$$\frac{\Delta h}{J_\perp} = 2\tilde{J}_{xy}^{(1)}[2(L-1)\tilde{\delta}^{(1)} - \tilde{g}^{(1)}], \quad (34)$$
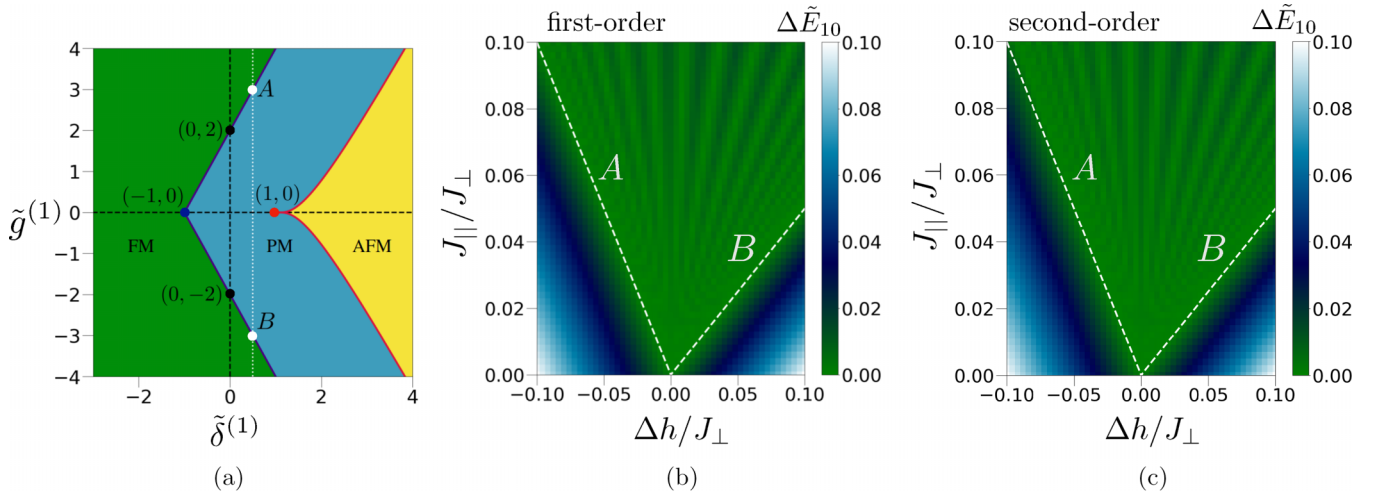

(a)

(b)

(c)

FIG. 4. (a) Phase diagram of the first-order 1D effective model [Eq. (25)] with $\tilde{J}_{xy} = 1$ and keeping L fixed at 2, on the plane of $(\tilde{\delta}^{(1)}, \tilde{g}^{(1)})$ [31,34,35], where the antiferromagnetic (AFM), ferromagnetic (FM), and paramagnetic (PM) phases and the corresponding phase boundaries are marked. For $J_d^{1,2} = 0$, the phase diagram truncates to the line $\tilde{\delta}^{(1)} = 1/2$, and the quantum phase transition from the gapless PM phase to the gapped FM phase takes place at the points $(\tilde{\delta}^{(1)} = 1/2, \tilde{g}^{(1)} = \pm 3)$, which we denote by A (for $\tilde{g}^{(1)} > 0$) and B (for $\tilde{g}^{(1)} < 0$). The variation of $\Delta\tilde{E}_{10}$ is plotted as functions of $J_{||}/J_\perp$ and $\Delta h/J_\perp$ in (b) and (c) keeping $J_d^{1,2} = 0$, where the $\Delta\tilde{E}_{10}$ is calculated using respectively (b) the first-order and (c) the second-order effective 1D Hamiltonian, as given in Eqs. (25) and (29) respectively, on an effective 1D lattice of $N = 20$ spins. The white dashed lines on the $(J_{||}/J_\perp, \Delta h/J_\perp)$ plane correspond to the points A and B, respectively, given by Eq. (36). All quantities plotted are dimensionless.

while for $L = 2$,

$$\frac{J_{||}}{J_{\perp}} = 2\tilde{J}_{xy}^{(1)}(2\tilde{\delta}^{(1)} + 1),$$

$$\frac{J_d^{\text{sum}}}{J_{\perp}} = 4\tilde{J}_{xy}^{(1)}(2\tilde{\delta}^{(1)} - 1),$$

$$\frac{\Delta h}{J_{\perp}} = 2\tilde{J}_{xy}^{(1)}[2\tilde{\delta}^{(1)} - \tilde{g}^{(1)}]. \tag{35}$$

Note that the appearance of $\tilde{J}_{xy}^{(1)}$ as a multiplicative factor in the above equations implies that the full phase diagram depicted in Fig. 4(a) is accessible in the perturbative regime of the 2D model H [Eq. (10)] by tuning $\tilde{J}_{xy}^{(1)}$, as long as $\tilde{J}_{xy}^{(1)} \neq 0$, and at least one of $J_d^1, J_d^2 \neq 0$. For $J_d^{1,2} = 0$ (i.e., $J_d^{\text{sum}} = 0$), the phase diagram truncates to the line $\tilde{\delta}^{(1)} = 1/L$ on the $(\tilde{\delta}^{(1)}, \tilde{g}^{(1)})$ plane for all values of L. On this line, a quantum phase transition from the gapless paramagnetic (PM) to the gapped ferromagnetic (FM) phase takes place by tuning $\tilde{g}^{(1)}$ at $\tilde{g}^{(1)} = \pm 2(L + 1)/L$. Note that these quantum phase transition points $(L^{-1}, \pm 2(L+1)/L)$ corresponding to $J_d^{1,2} = 0$ translates to the lines

$$\frac{\Delta h}{J_{\perp}} = \frac{2J_{||}}{J_{\perp}},$$

$$\frac{\Delta h}{J_{\perp}} = \frac{-2J_{||}}{LJ_{\perp}}, \tag{36}$$

for all even values of L on the $(J_{||}/J_{\perp}, \Delta h/J_{\perp})$ plane in the parameter space of the original model. In Fig. 4(b) we plot the energy gap $\Delta\tilde{E}_{10} = \tilde{E}_1 - \tilde{E}_0$ as a function of the system parameters of the 2D model, *viz.* $J_{||}/J_{\perp}$ and $\Delta h/J_{\perp}$, in the perturbation regime [Eq. (32)] for $J_d^{1,2} = 0$ and $L = 2$, where $\tilde{E}_0$ and $\tilde{E}_1$ are the ground and the first excited state energies corresponding to the Hamiltonian $\tilde{H}$ [Eq. (25)]. The lines in Eq. (36) are also presented for reference. Note that Fig. 4(b) provides the phase diagram of the gapped and the gapless phases of the 2D model with $L = 2$ and $J_d^{1,2} = 0$. In a similar fashion, the gapped and the gapless phases of the 2D model for different values of $L(> 2)$ can be mapped when the system parameters are kept within the perturbation regime. Also, using a similar approach, one can investigate the phase diagram on the $(J_{||}/J_{\perp}, \Delta h/J_{\perp})$ for different nonzero values of J_d^{sum} (or, J_d^1 and J_d^2); see Sec. III.

Note that the maximum value of $\tilde{\delta}^{(1)}$ occurs for the two-leg ladder ($L = 2$) discussed above and in Fig. 4(b), while $\tilde{\delta}^{(1)} \rightarrow 0$ in the *large L limit*. We point out here that in the large L limit [but obeying Eq. (31)], the effective 1D model is an XX model in a transverse magnetic field [36], represented by the Hamiltonian

$$\tilde{H} = \tilde{J}_{xy}^{(1)} \sum_{i=1}^{N} \left[\left(\tau_i^x \tau_{i+1}^x + \tau_i^y \tau_{i+1}^y \right) + \tilde{g}^{(1)} \tau_i^z \right], \tag{37}$$

which can be exactly solved via fermionization using the Jordan-Wigner transformation, followed by a Fourier transformation. The phase diagram of this model has been extensively explored, showing a second-order quantum phase transition at $\tilde{g}^{(1)} = \pm 2$ from the PM phase to the FM phase for $\tilde{J}_{xy}^{(1)} = 1$ [see $\tilde{\delta}^{(1)} = 0$ line in Fig. 4(a)].

2. Phase information from the second-order effective Hamiltonian

It is now logical to ask whether additional information can be obtained about the phase diagram of the 2D model via considering the perturbation theory up to the second order. In order to explore this, we set $J_d^{1,2} = 0$ (i.e., $J_d^{\text{sum}} = 0$), such that Eqs. (29) and (30) exhaust all even values of L. One can also keep $J_d^{1,2} \neq 0$, and treat the $L = 2$ case separately. However, we choose $J_d^{1,2} = 0$ in order to work with Eqs. (29) and to avoid involving more effective Hamiltonian parameters [see Eqs. (A12) and (A18) in the Appendix].

Note that $\tilde{\gamma}^{(2)}$ is introduced solely due to the second-order correction, and since $\tilde{\gamma}^{(2)} > 0$ for a nonzero value of $J_{||}$, the $\tilde{\gamma}^{(2)} = 0$ plane in the $(\tilde{g}^{(2)}, \tilde{\delta}^{(2)}, \tilde{\gamma}^{(2)})$ parameter space is never accessible via the second-order effective Hamiltonian. Note further that $\tilde{\delta}^{(2)}$ and $\tilde{g}^{(2)}$ can be written as

$$\tilde{\delta}^{(2)} = \tilde{\delta}^{(1)} + \tilde{F},$$

$$\tilde{g}^{(2)} = \tilde{g}^{(1)} + \tilde{G}, \tag{38}$$

where we identify $\tilde{\delta}^{(1)}$ and $\tilde{g}^{(1)}$ from the first-order calculation with $J_d^{1,2} = 0$, and

$$\tilde{F} = \frac{1}{2}\left(\frac{J_{||}}{J_{\perp}}\right)F + \left(\frac{J_{\perp}}{J_{||}}\right)G,$$

$$\tilde{G} = -\frac{1}{2}\left(\frac{J_{||}}{J_{\perp}}\right)F - 2\left(\frac{J_{\perp}}{J_{||}}\right)G \tag{39}$$

to be the contribution solely from the second-order calculation. For a fixed $\tilde{\gamma}^{(2)}$ (i.e., for a fixed $J_{||}/J_{\perp}$), $\tilde{F}$ and $\tilde{G}$ depend only on L, and within the range of parameters considered in this paper [see Eqs. (32) and (33)], $\tilde{F}$ leads to a very small perturbatively allowed window around $\tilde{\delta}^{(1)}$. Therefore, for a fixed value of L and $J_{||}$, one expects the phases of the system to be ploughed by $\tilde{g}^{(2)}$, and the phase diagram to be similar to that corresponding to the $\tilde{\delta}^{(1)} = L^{-1}$ line of Fig. 4. For example, consider the case of $L = 2$ with fixing $J_{\perp} = 1$, which we employ for demonstrating our inferences, such that $\tilde{\delta}^{(1)} = 1/2$, and $\Delta E(L) = 1$, with the considered range $[0,0.1]$ of the perturbation parameters, which yields $0 \leqslant \tilde{F} \leqslant 0.075$. In support of these points, in Fig. 4(c), we plot $\Delta\tilde{E}_{10}$ computed from the second-order $\tilde{H}$ [Eq. (29)] as functions of $J_{||}/J_{\perp}$ and $\Delta h/J_{\perp}$, keeping $J_d^{1,2} = 0$ and $L = 2$. The boundaries of the gapped and the gapless phase obtained from this figure, along with the values of $\Delta\tilde{E}_{10}$, are almost identical with the same obtained from the first-order theory, as shown in Fig. 4(b), thereby supporting our analysis. We point out here that one can also perform the analysis with $J_d^{1,2} \neq 0$ and satisfying Eq. (31), where similar arguments hold.

Similar to the first-order case, here also in the limit $L \rightarrow \infty$, both F and $G \rightarrow 0$, leading to $\tilde{\delta}^{(2)} = 0$, and $\tilde{g}^{(2)} \approx 2[1 - \Delta h/J_{||}]$, where the effective 1D Hamiltonian becomes

$$\tilde{H} = \tilde{J}_{xy}^{(2)}\left[\sum_{i=1}^{N} \left(\tau_i^x \tau_{i+1}^x + \tau_i^y \tau_{i+1}^y \right) + \tilde{g}^{(2)} \sum_{i=1}^{N} \tau_i^z \right.$$

$$\left. + \tilde{\gamma}^{(2)} \sum_{i=1}^{N} \left(\tau_{i-1}^x \tau_{i+1}^x + \tau_{i-1}^y \tau_{i+1}^y \right)\left(I_i - \tau_i^z \right) \right]. \tag{40}$$

Similar to $\tilde{H}$ in Eq. (37), the above 1D Hamiltonian can be exactly solved using a Jordan-Wigner, and subsequently a

Fourier, transformation, leading to a phase diagram involving two spin liquid and an FM phase [37]. Since the value of $\tilde{\gamma}^{(2)}$ is small for perturbation theory to be valid, we expect the phase features to be remain same for the first- and the second-order effective Hamiltonian around the line $\tilde{\delta}^{(2)} = 0$.

III. BEYOND THE PERTURBATION REGIME

In this section we investigate the performance of the 1D effective theory in estimating properties of the 2D model even beyond the perturbation regime, focusing primarily on the energy gap, expectation values of Hermitian operators, and entanglement [9]. Perturbation theory up to second order in the parameter $J_\perp^{-1}$ leads to the following structure for the energy eigenvalues $\{E_l, l = 0, 1, \ldots, 2^{NL} - 1\}$ and the corresponding eigenstates $\{|\Phi_l\rangle\}$ of the 2D model:

$$E_l = E_l^{(0)} + J_\perp^{-1} E_l^{(1)} + J_\perp^{-2} E_l^{(2)} + O(J_\perp^{-3}),$$

$$|\Phi_l\rangle = |\Phi_l^{(0)}\rangle + J_\perp^{-1}|\Phi_l^{(1)}\rangle + O(J_\perp^{-2}), \quad (41)$$

Diagonalization of the second-order $\tilde{H}$ given in Eq. (14) provides $J_\perp^{-1} E_l^{(1)} + J_\perp^{-2} E_l^{(2)}$ (note that we have ensured $E_l^{(0)} = 0$; see Secs. II A and II B) as the energy eigenvalues, and $|\Phi_l^{(0)}\rangle + J_\perp^{-1}|\Phi_l^{(1)}\rangle$ as energy eigenstates. It is worthwhile to note that the energy eigenstates $|\tilde{\Phi}_l\rangle$ of the effective second-order 1D model $\tilde{H}$ [Eq. (29)], given by $\tilde{H}|\tilde{\Phi}_l\rangle = \tilde{E}_l|\tilde{\Phi}_l\rangle$ with $\tilde{E}_l = J_\perp^{-1} E_l^{(1)} + J_\perp^{-2} E_l^{(2)}$, can be written in terms of $\{|\mathbf{0}\rangle, |\mathbf{1}\rangle\}$, and provides $|\Phi_l^{(0)}\rangle + J_\perp^{-1}|\Phi_l^{(1)}\rangle$, i.e., $|\Phi_l\rangle$ up to $O(J_\perp^{-2})$ when expanded using the definitions of $|\psi_{0,1}\rangle$.

We are particularly interested in the ground states of both models, which can, in principle, be degenerate depending on the choice of the parameter values in the ranges considered in Eqs. (32) and (33). We assume respectively M-, and $\tilde{M}$-fold degenerate ground state manifolds $\{|\Phi_l\rangle\}, l = 0, \ldots, M - 1\}$ and $\{|\tilde{\Phi}_l\rangle\}, l = 0, \ldots, \tilde{M} - 1\}$ corresponding respectively to the ground state energies E_0 and $\tilde{E}_0$ of the 2D model[1] and the second-order 1D effective model [Eq. (29)]. To avoid subtleties such as the choice of the state among the degenerate ground state manifold for computing the quantity of interest, we consider the *thermal ground states* [38] as

$$\rho_0 = M^{-1} \sum_{l=0}^{M-1} |\Phi_l\rangle\langle\Phi_l|, \quad (42)$$

$$\tilde{\varrho}_0 = \tilde{M}^{-1} \sum_{l=1}^{\tilde{M}-1} |\tilde{\Phi}_l\rangle\langle\tilde{\Phi}_l|, \quad (43)$$

which are obtained by considering a thermal state at the zero temperature limit. Converting $\tilde{\varrho}_0$ to a state ϱ_0 in the Hilbert space of the 2D model using the definitions of $|\psi_{0,1}\rangle$, we compute the trace distance D between ρ_0 and ϱ_0 as

$$D = \frac{1}{2}\text{Tr}\sqrt{(\rho_0 - \varrho_0)^\dagger (\rho_0 - \varrho_0)}. \quad (44)$$

---

[1]The values of M and $\tilde{M}$ depend on the choice of the system parameters $J_\parallel/J_\perp$, $J_d^{1,2}/J_\perp$, and $\Delta h/J_\perp$. For all the points in the parameter space $(J_\parallel/J_\perp, \Delta h/J_\perp)$ considered in Fig. 5 with $J_d^{1,2} = 0$, we find $M = \tilde{M}$.

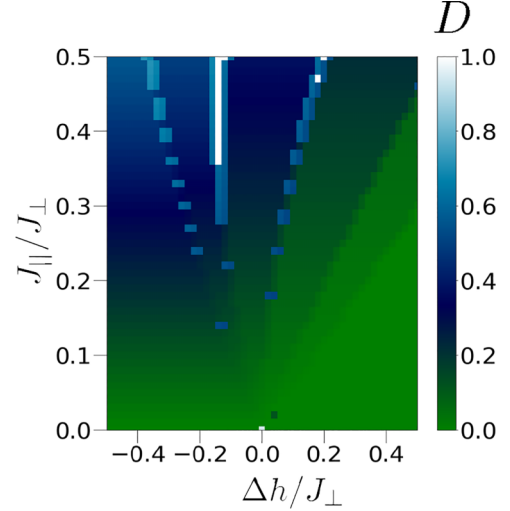FIG. 5. Variation of D as a function of $J_\parallel/J_\perp$ and $\Delta h/J_\perp$ outside the perturbation regime with $J_d^{1,2} = 0$. A lattice of size 6×2 has been used for computation. All quantities plotted are dimensionless.

The variation of D as a function of $J_\parallel/J_\perp$ and $\Delta h/J_\perp$ with $J_d^{1,2} = 0$ is plotted in Fig. 5. Our data indicate that inside the perturbation regime [Eq. (32) with $J_d^{1,2} = 0$], as expected, $D \sim 0$, while outside the perturbation regime [Eq. (33) with $J_d^{1,2} = 0$], $D > 0$. It is, therefore, expected that a physical quantity whose evaluation requires information about the thermal ground state away from the perturbation regime would be difficult to estimate using the effective 1D theory. We will revisit this point as we discuss the evaluation of energy gap, expectation values of Hermitian operators, and entanglement in the subsequent subsections.

A. Energy gap

We first consider the energy gap $\Delta E_{ll'} = E_l - E_{l'}$ between two low-lying states (l and l') of the original model H, given by [see Eq. (41)]

$$\Delta E_{ll'} = J_\perp^{-1} \Delta E_{ll'}^{(1)} + J_\perp^{-2} \Delta E_{ll'}^{(2)} + O(J_\perp^{-3}), \quad (45)$$

with $\Delta E_{ll'}^{(i)} = E_l^{(i)} - E_{l'}^{(i)}$, $i = 1, 2$. Note that $\Delta E_{ll'}$ is almost the same as $\Delta \tilde{E}_{ll'} = \tilde{E}_l - \tilde{E}_{l'}$ up to $O(J_\perp^{-3})$ obtained from the second-order effective Hamiltonian $\tilde{H}$ [Eq. (29)] as long as the perturbation theory is valid [i.e., the system parameters obey Eq. (31)]. We would, however, like to check *if $\Delta \tilde{E}_{ll'}$ faithfully represents $\Delta E_{ll'}$ when the system parameters are chosen from beyond the perturbation regime*. In Figs. 6(a) and 6(b), we plot the variations of respectively $\Delta E_{10} = E_1 - E_0$ and $\Delta \tilde{E}_{10} = \tilde{E}_1 - \tilde{E}_0$ as functions of $J_\parallel/J_\perp$ and $\Delta h/J_\perp$ with $J_d^1 = J_d^2 = 0$, where the range of values of $J_\parallel/J_\perp$ and $\Delta h/J_\perp$ include both Eqs. (32) and (33). Here E_l and $\tilde{E}_l$ are computed via exact diagonalization (ED) respectively from the 2D model H [Eq. (1)] over a 20-qubit system on a 10×2 lattice, and from the second-order $\tilde{H}$ [Eq. (29)] defined on a 1D lattice of 10 spins. It is clear from the Figs. 6(a) and 6(b) that the landscape ΔE_{10} of the actual model is imitated qualitatively as well as quantitatively by $\Delta \tilde{E}_{10}$ obtained from the second-order effective model, even for almost all points outside the parameter space where perturbation theory is valid. Similar
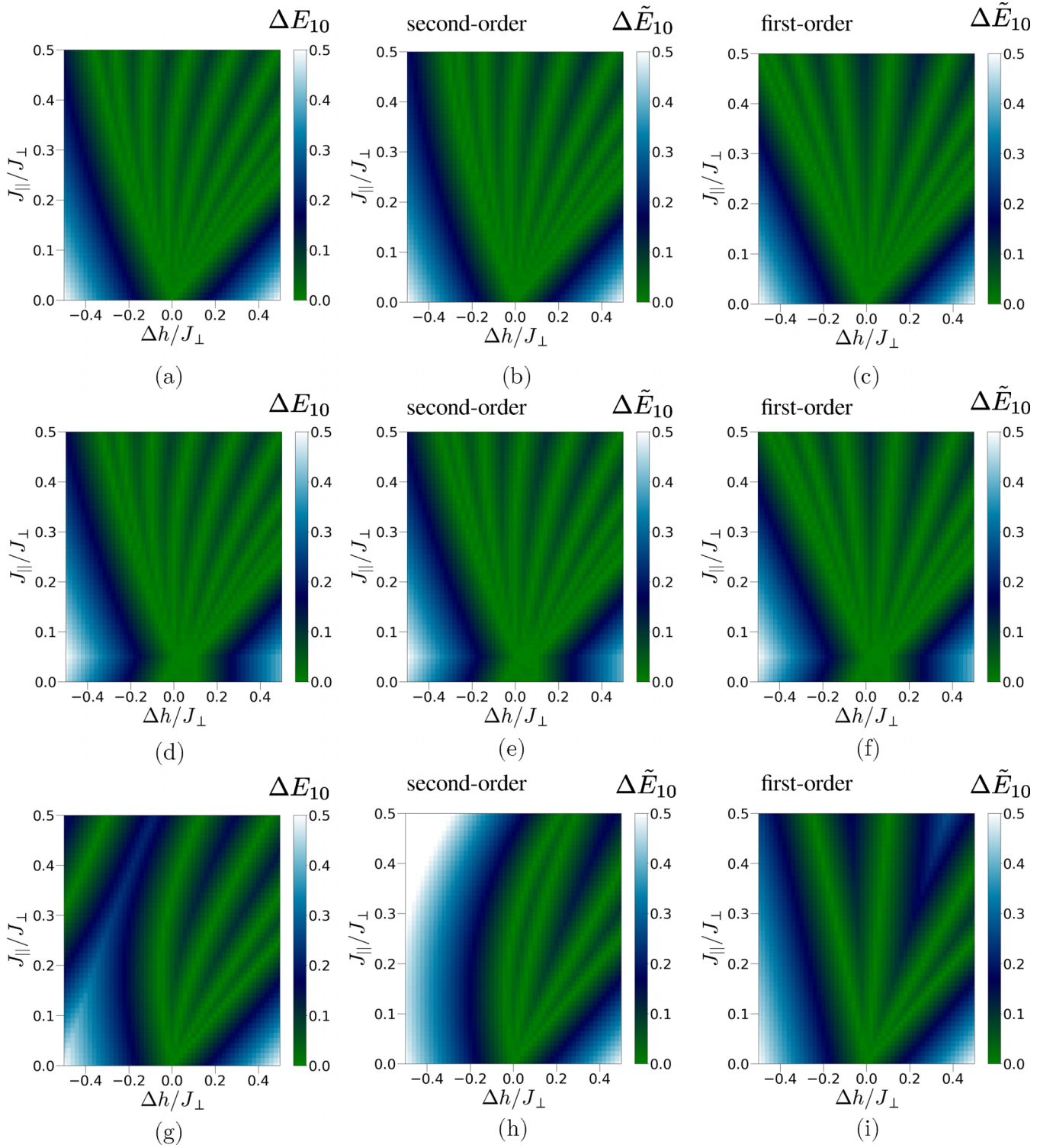
FIG. 6. Variations of the energy gap ΔE_{10} obtained from H on a 10×2 (20 qubits) 2D lattice with (a–c) $J_d^{1,2} = 0$ and (d–f) $J_d^{1,2} = 5 \times 10^{-2}$ as functions of $J_{\parallel}/J_{\perp}$ and $\Delta h/J_{\perp}$ outside the perturbation regime. The corresponding $\Delta \tilde{E}_{10}$ obtained from the (b, e) second-order effective Hamiltonian $\tilde{H}$ [Eq. (29)], and the same obtained from (c, f) the first-order effective Hamiltonian $\tilde{H}$ [Eq. (25)], both defined on a chain of 10 spins, as functions of $J_{\parallel}/J_{\perp}$ and $\Delta h/J_{\perp}$ outside the perturbation regime, are depicted in (b), (e), (c), and (f). Similar plots for a lattice of 16 spins (4×4) are given in (g), (h), and (i) for $J_d^{1,2} = 0$, while nonzero values of $J_d^{1,2}$ produce qualitatively similar results. All quantities plotted are dimensionless.

TABLE I. Typical observables A on the 2D model and the corresponding low-energy components $\tilde{A}$, i.e., $A_{\mathcal{S}}$ [Eq. (48)] in terms of $\tau^{x,y,z}$, where PBC along both rungs and legs have been used for calculation. A subset of these operators for $L = 2$ can be found in [26]. Note that $\tilde{A}$ corresponding to $\sigma^\alpha_{i,j}$, $\alpha = x, y, z$, is consistent with the operator identification of J^z_i in terms of τ^z_i, as given in Eqs. (20) and (17). Among these operators, Eq. (49) is satisfied for $\sum_{j=1}^L \sigma^z_{i,j}$ (No. 3) and $\otimes_{j=1}^L \sigma^z_{i,j}$ (No. 6). More of such operators can be constructed on the 2D model by considering these operators on different rungs; for example, $A = (\sum_{j=1}^L \sigma^z_{i,j}) \otimes (\sum_{j=1}^L \sigma^z_{i+r,j})$ is also an operator satisfying Eq. (49), having support on the rungs i and $i + r$.

No.	A	$\tilde{A} (\equiv A_{\mathcal{S}})$	No.	A	$\tilde{A} (\equiv A_{\mathcal{S}})$
1	$\sigma^\alpha_{i,j}$	$\frac{(-1)^j}{\sqrt{L}} \tau^\alpha_i$, for $\alpha = x, y$	12	$\sigma^z_{i,1} \otimes \sigma^y_{i,2}$	$\frac{1}{\sqrt{2}} \tau^y_i$
2	$\sigma^z_{i,j}$	$\frac{L-1}{L} I_i + \frac{1}{L} \tau^z_i$	13	$\sigma^x_{i,1} \otimes \sigma^y_{i,2}$	0
3	$\sum_{j=1}^L \sigma^z_{i,j}$	$(L-1)I_i + \tau^z_i$	14	$\sigma^y_{i,1} \otimes \sigma^x_{i,2}$	0
4	$\sum_{j=1}^L \sigma^x_{i,j}$	0	15	$\sigma^\alpha_{i,j} \otimes \sigma^\alpha_{i+r,j'}$	$\frac{(-1)^{j+j'}}{L} \tau^\alpha_i \otimes \tau^\alpha_{i+r}$ for $\alpha = x, y$
5	$\sum_{j=1}^L \sigma^y_{i,j}$	0	16	$\sigma^z_{i,j} \otimes \sigma^z_{i+r,j'}$	$\frac{(L-1)^2}{L^2} I + \frac{1}{L^2} \tau^z_i \tau^z_{i+r} + \frac{L-1}{L^2}(\tau^z_i + \tau^z_{i+r})$
6	$\otimes_{j=1}^L \sigma^z_{i,j}$	τ^z_i	17	$\sigma^x_{i,j} \otimes \sigma^z_{i+r,j'}$	$\frac{(-1)^j}{\sqrt{L}}[\frac{L-1}{L} \tau^x_i + \frac{1}{L} \tau^x_i \tau^z_{i+r}]$
7	$\otimes_{j=1}^L \sigma^x_{i,j}$	$\begin{pmatrix} \frac{1}{2}(\tau^z_i - I_i) & \text{for } L = 2 \\ 0 & \text{for } L > 2 \end{pmatrix}$	18	$\sigma^z_{i,j} \otimes \sigma^x_{i+r,j'}$	$\frac{(-1)^{j'}}{\sqrt{L}}[\frac{L-1}{L} \tau^x_{i+r} + \frac{1}{L} \tau^z_i \tau^x_{i+r}]$
8	$\otimes_{j=1}^L \sigma^y_{i,j}$	$\begin{pmatrix} \frac{1}{2}(\tau^z_i - I_i) & \text{for } L = 2 \\ 0 & \text{for } L > 2 \end{pmatrix}$	19	$\sigma^y_{i,j} \otimes \sigma^z_{i+r,j'}$	$\frac{(-1)^j}{\sqrt{L}}[\frac{L-1}{L} \tau^y_i + \frac{1}{L} \tau^y_i \tau^z_{i+r}]$
9	$\sigma^x_{i,1} \otimes \sigma^z_{i,2}$	$-\frac{1}{\sqrt{2}} \tau^x_i$	20	$\sigma^z_{i,j} \otimes \sigma^y_{i+r,j'}$	$\frac{(-1)^{j'}}{\sqrt{L}}[\frac{L-1}{L} \tau^y_{i+r} + \frac{1}{L} \tau^z_i \tau^y_{i+r}]$
10	$\sigma^z_{i,1} \otimes \sigma^x_{i,2}$	$\frac{1}{\sqrt{2}} \tau^x_i$	21	$\sigma^x_{i,j} \otimes \sigma^y_{i+r,j'}$	0
11	$\sigma^y_{i,1} \otimes \sigma^z_{i,2}$	$-\frac{1}{\sqrt{2}} \tau^y_i$	22	$\sigma^y_{i,j} \otimes \sigma^x_{i+r,j'}$	0

analysis for nonzero values of the diagonal interactions $J^{1,2}_d$, with $J^1_d = J^2_d = 5 \times 10^{-2}$, on a 10×2 lattice is presented in Figs. 6(d)–6(f), indicating a similar inference. In order to see if this observation holds for 2D lattices with $L > 2$, we perform similar investigations for a 4×4 lattice, and present the results in Figs. 6(g)–6(i) for $J^{1,2}_d = 0$, while nonzero values of $J^{1,2}_d$ produce qualitatively similar results. Our data clearly indicate that in addition to the perturbation regime, given by [see Eq. (32)]

$$0 \leqslant J_{||}/J_\perp, |\Delta h/J_\perp|, J^{1,2}_d/J_\perp \leqslant 0.1, \quad (46)$$

there exists points outside the perturbation regime on which the 1D effective model up to second order estimates the energy gap of the 2D model with $L = 4$ satisfactorily. However, the validity of this observation at different parameter space point outside the perturbation regime and for different values of L needs to be tested in a case-by-case basis.

B. Expectation values of Hermitian operators

We now consider Hermitian operators in the 2D Heisenberg model, and discuss estimation of their expectation values in the low-energy manifold of H using the representation of the manifold via the effective 1D model. We first stress the following points regarding the notations used in the rest of the paper.

(a) Each operator A defined on the Hilbert space of the 2D model can be decomposed as

$$A = P_g A P_g + P_e A P_e + P_g A P_e + P_e A P_g, \quad (47)$$

where the projector P_g [Eq. (9)] projects an operator onto the low-energy subspace $\mathcal{S}$ (see Secs. II A and II B). We denote

$$A_{\mathcal{S}} = P_g A P_g, \quad (48)$$

and note that $A_{\mathcal{S}}$ can be thought of as an operator on the Hilbert space of the 1D effective model representing the *low-energy component* of A. We typically denote such operators, when written in terms of $\tau^{x,y,z}$ by $\tilde{A}$. Also, we call all operators with

$$P_g A P_e = P_e A P_g = 0 \quad (49)$$

low-energy operators.

(b) These details also apply to a state ρ of the 2D model, which is a Hermitian operator. However, in the case of density matrices, we are interested only in states for which $P_e \rho P_e = P_g \rho P_e = P_e \rho P_g = 0$. We call them *low-energy density matrices*. Note that both the states ρ_0 [Eq. (42)] and ϱ_0 obtained from $\tilde{\varrho}_0$ [Eq. (43)] are low-energy density matrices.

We consider a number of relevant operators A on the space of the 2D model (see Table I), and determine (a) the corresponding $A_{\mathcal{S}}$, and (b) their closed forms in terms of $\tau^{x,y,z}$, denoted by $\tilde{A}$. Note that the expectation value of any operator w.r.t. a low-energy density matrix ρ is given by

$$\langle A \rangle = \text{Tr}(\rho A) = \text{Tr}(\rho A_{\mathcal{S}}), \quad (50)$$

which equals $\langle \tilde{A} \rangle = \text{Tr}(\tilde{A}\tilde{\varrho})$ up to $O(J^{-3}_\perp)$ in the perturbation regime of the parameter space, where $\tilde{\varrho}$ provides the first-order approximation of ρ obtained using the second-order 1D effective Hamiltonian (our numerical analysis performed on moderate-sized systems confirms this). Since computation of $\langle A \rangle$ for the 2D model is difficult owing to the large Hilbert space dimension, this provides a computational advantage in estimating $\langle A \rangle$ using $\langle \tilde{A} \rangle$, and subsequently the second-order 1D effective Hamiltonian.

We are, however, interested in exploring whether this advantage persists even beyond the realm of perturbation theory, i.e., *whether $\langle \tilde{A} \rangle$ can mimic $\langle A \rangle$ when the system parameters are chosen outside the perturbation regime*. We answer this
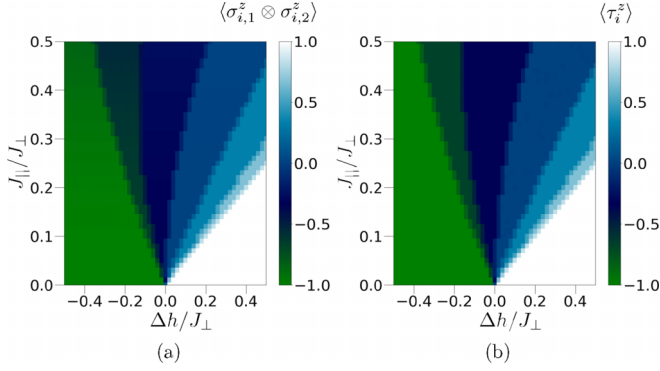
FIG. 7. Variations of (a) $\langle A \rangle$ and (b) $\langle \tilde{A} \rangle$ as functions of $J_{||}/J_\perp$ and $\Delta h/J_\perp$ outside the perturbation regime, with $J_d^{1,2} = 0$, where $A = \sigma_{i,1}^z \otimes \sigma_{i,2}^z$. We use a 6×2 lattice for computing $\langle A \rangle$, while $\langle \tilde{A} \rangle$ is computed for a 1D lattice of six effective spins. All quantities plotted are dimensionless.

question affirmatively for the class of low-energy operators [see Eq. (49)]. To demonstrate this, we choose the low-energy operators $A = \otimes_{j=1}^L \sigma_{i,j}^z$ listed in Table I in the case of $L = 2$, and compute $\langle A \rangle = \mathrm{Tr}(\rho_0 A_\mathcal{S})$ and $\langle \tilde{A} \rangle = \mathrm{Tr}(\tilde{\varrho}_0 \tilde{A})$, where ρ_0 and $\tilde{\varrho}_0$ are given in Eqs. (42) and (43) respectively. Variations of $\langle A \rangle$ and $\langle \tilde{A} \rangle$ as functions of $J_{||}/J_\perp$ and $\Delta h/J_\perp$ (with $J_d^{1,2} = 0$), computed for a system of 12 spins on a 6×2 lattice, are depicted in Figs. 7(a) and 7(b), respectively. The figures clearly indicate that outside the perturbation regime of the parameter space (where $D > 0$; see Fig. 5), $\langle \tilde{A} \rangle$ mimics $\langle A \rangle$.

C. Entanglement

We now extend the discussion towards nonlocal correlations that are properties of a multiqubit quantum states, e.g., entanglement [9]. While the distribution of entanglement in a quantum spin model can be varied, such as bipartite and multipartite entanglement over different subsystems, it often adapts a partial trace-based methodology for computation [9]. For example, the bipartite entanglement between two subsystems constituting a bipartite system in a pure state is inferred from the reduced density matrix of one of the subsystems obtained by tracing out the other subsystem from the pure state. As examples, we choose ρ_0 and $\tilde{\varrho}_0$ for discussions. The reduced density matrix $\rho_{0,i}$ obtained by tracing out all rungs except the rung i from ρ_0, and the reduced density matrix $\tilde{\varrho}_{0,i}$ obtained from $\tilde{\varrho}_0$ by tracing out all spins except the spin corresponding to i are equal up to $O(J_\perp^{-3})$ (see Sec. II E), i.e., $\rho_{0,i} - \varrho_{0,i} = O(J_\perp^{-3})$, where $\varrho_{0,i}$ is obtained from $\tilde{\varrho}_{0,i}$ by using the definitions of $|\psi_{0,1}\rangle$.[2] This implies that any entanglement measure [9] E computed from these density matrices are expected to match, although the difference between $E(\rho_{0,i})$ and $E(\tilde{\varrho}_{0,i})$ depends on the explicit functional form E, and
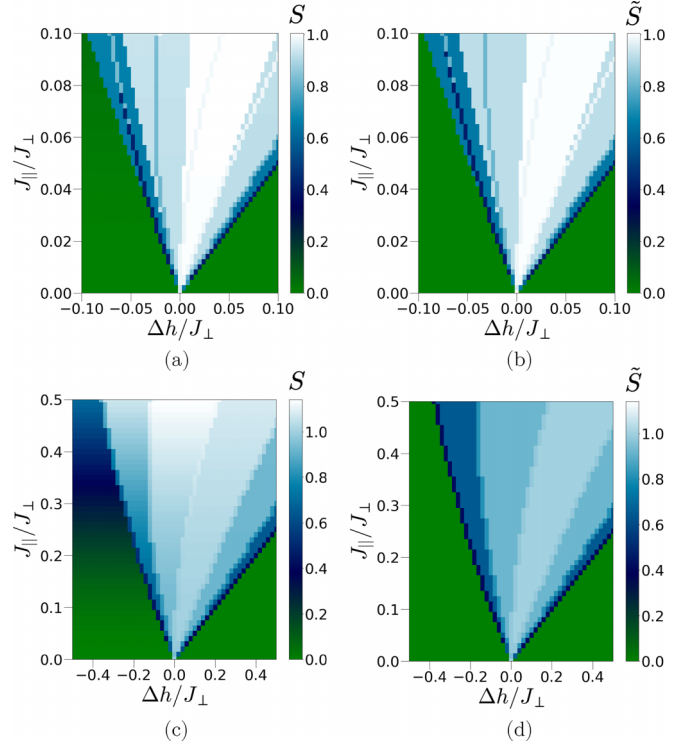

FIG. 8. Variations of (a) S and (b) $\tilde{S}$ in the perturbation regime, and the same outside the perturbation regime (c, d) as functions of $J_{||}/J_\perp$ and $\Delta h/J_\perp$ with $J_d^{1,2} = 0$. For computation of S, we determine ρ_0 for a 2D lattice of size 6×2, while $\tilde{S}$ is computed on a chain of effective spins of size 6. All quantities plotted are dimensionless.

an accumulation of factors $O(J_\perp^{-3})$ may also take place giving rise to a higher difference. For demonstration, we compute von Neumann entropy [9,39] S and $\tilde{S}$ of the reduced density matrices $\tilde{\varrho}_{0,i}$ and $\rho_{0,i}$ respectively.[3] For an arbitrary density matrix ρ, it is computed as

$$S(\rho) = -\mathrm{Tr}[\rho \log_2 \rho] = -\sum_i \lambda_i \log_2 \lambda_i, \qquad (51)$$

where $\{\lambda_i\}$ is the set of eigenvalues of ρ. In Figs. 8(a) and 8(b) we respectively plot S and $\tilde{S}$ as functions of $J_{||}/J_\perp$ and $\Delta h/J_\perp$ within the perturbation regime, with $J_d^{1,2} = 0$. It is evident from the figures that $\tilde{S}$ can faithfully represent S in the perturbation regime.

We further consider the two-rung reduced density matrix $\rho_0^{(i,i')}$ over the rungs i and $i' = i + 1$ in the 2D model, and the corresponding two-spin density matrix $\tilde{\varrho}_0^{(i,i')}$ in the 1D effective model, and compute negativity [40], denoted by $\mathcal{N}$ and $\tilde{\mathcal{N}}$ respectively, quantifying bipartite entanglement between the rungs (spins) i and $i' = i + 1$. For an arbitrary density matrix

---

[2]One can also extend it further to the reduced density matrix of a subsystem composed of a set of arbitrary number of rungs obtained from the state ρ_0 of the 2D model H, and the reduced density matrix of the corresponding set of spins obtained from the state $\tilde{\varrho}_0$ of the 1D effective model $\tilde{H}$ [Eq. (28)].

[3]Von Neumann entropy of the reduced density matrix of a rung (an effective spin) in the 2D model (effective 1D model) quantifies entanglement between the rung (spin) and the rest of the system if the original state of the full system is pure. While it is not the situation in the present case, it is sufficient to consider von Neumann entropy function for discussion.
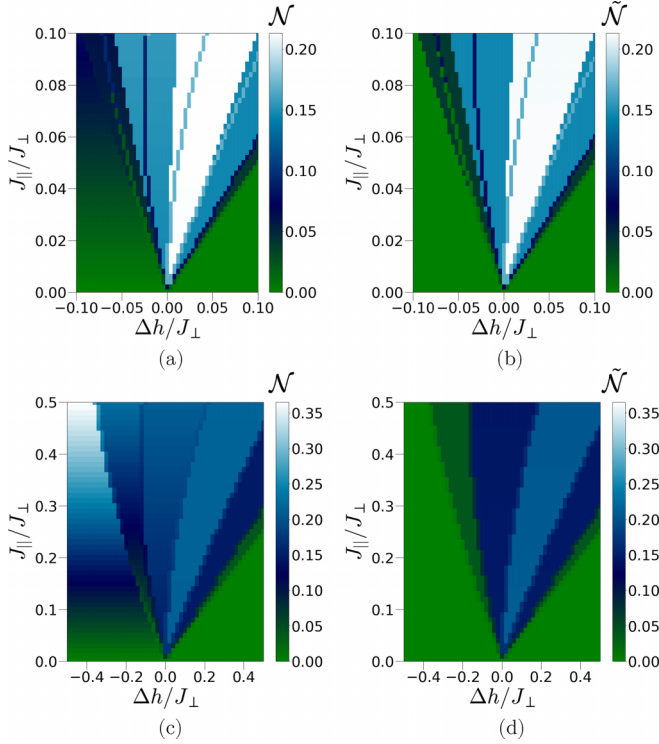
FIG. 9. Variations of (a) $\mathcal{N}$ and (b) $\tilde{\mathcal{N}}$ in the perturbation regime, and the same outside the perturbation regime (c, d) as functions of $J_{||}/J_\perp$ and $\Delta h/J_\perp$ with $J_d^{1,2} = 0$. The system sizes and states are the same as in Fig. 8. All quantities plotted are dimensionless.

ρ for a composite quantum system constituted of two parties A and B, negativity is defined as

$$\mathcal{N}(\rho) = \sum_i |\lambda_i|, \tag{52}$$

where $\{\lambda_i\}$ is the set of all negative eigenvalues of the partially transposed density matrix ρ^{T_A}, the partial transposition being taken w.r.t. the subsystem A. In the present case, we identify the two rungs (spins) as the two subsystems. In Figs. 9(a) and 9(b) we respectively plot $\mathcal{N}$ and $\tilde{\mathcal{N}}$ as functions of $J_{||}/J_\perp$ and $\Delta h/J_\perp$ within the perturbation regime, with $J_d^{1,2} = 0$. It is evident from the figures that $\tilde{\mathcal{N}}$ can faithfully represent $\mathcal{N}$ in the perturbation regime.

However, unlike the expectation values of low-energy operators, $E(\tilde{\varrho}_{0,i})$ fails to represent $E(\rho_{0,i})$ outside the perturbation regime. This can be understood from the fact that the density matrix $\rho_{0,i}$ corresponding to the rung i can be decomposed in terms of Pauli matrices as

$$\rho_{0,i} = \frac{1}{2^L} \sum_{\{\alpha_j\}} c_{\{\alpha_j\}} \left[\otimes_{j=1}^L \sigma_{i,j}^{\alpha_j}\right], \tag{53}$$

where $\sigma^{\alpha_j} \alpha_j = 0, 1, 2, 3$ correspond respectively to the operators I, σ^x, σ^y, and σ^z respectively, and

$$c_{\{\alpha_j\}} = \text{Tr}\left[\rho_{0,i}\left(\otimes_{j=1}^L \sigma_{i,j}^{\alpha_j}\right)\right]. \tag{54}$$

Since Eq. (48) is not satisfied for a subset of the operators $A = \otimes_{j=1}^L \sigma_{i,j}^{\alpha_j}$, outside the perturbation regime $\tilde{\varrho}_{0,i}$ (and subsequently $\varrho_{0,i}$) fails to mimic $\rho_{0,i}$, resulting in a considerable difference between $E(\tilde{\varrho}_{0,i})$ and $E(\rho_{0,i})$. We demonstrate this

by plotting S and $\tilde{S}$ in Figs. 8(c) and 8(d), and $\mathcal{N}$ and $\tilde{\mathcal{N}}$ in Figs. 9(c) and 9(d) respectively as functions of $J_{||}/J_\perp$ and $\Delta h/J_\perp$ outside the perturbation regime, with $J_d^{1,2} = 0$, where the differences between S and $\tilde{S}$, and between $\mathcal{N}$ and $\tilde{\mathcal{N}}$ are evident from the figures.

IV. CONCLUSION AND OUTLOOK

In this paper, we consider a spin-$1/2$ isotropic Heisenberg model in a magnetic field on a rectangular zig-zag lattice of arbitrary size $N \times L$. We show that irrespective of the values of N and L, the low-energy manifold of the 2D model in the strong-rung-coupling limit can be well approximated by a 1D effective spin-$1/2$ XXZ model up to the first order in perturbation theory, while using the second-order perturbation theory, the manifold is represented by the 1D effective spin-$1/2$ XXZ model with specific three-body interactions. We use this mapping to determine the phase diagram of the 2D model in the strong-rung-coupling limit, and calculate the energy gap, operator expectation values, and the von Neumann entropy in the 2D model. Also, we analytically determine the low-energy components of a number of Hermitian operators defined on the Hilbert space of the 2D model with arbitrary system size. Further we go beyond the perturbation regime of the parameter space, and show that the energy gap of the 2D model can be quantitatively represented by the same in the case of the 1D model even away from the strong-rung-coupling limit. Also, for a specific class of operators, the *low-energy operators*, we show that their expectation values in the states belonging to the low-energy subspace of the 2D model can be mimicked satisfactorily by the second-order 1D effective model. While these class of observables can be faithfully mimicked by the 1D theory outside the perturbation regime, we argue that it is not possible to do so for nonlocal correlations such as entanglement present in the low-lying states of the 2D model.

We conclude with a discussion on possible future works. While we focus on correlation functions and entanglement in this work, it would be interesting to explore the implication of the mapping of the 2D model to an effective 1D model in specific quantum information theoretic protocols, such as quantum state transfer [6,41]. Also, an interesting direction would be to generalize the calculation where ground states of individual rungs have higher degeneracies ($d > 2$), so that 2D models with d degrees of freedom per cite can be addressed. It is also important to ask whether expectation values of Hermitian operators defined on the 2D model for specific purposes, such as order parameters [42], or entanglement witness operators [43], can be estimated using the effective 1D model. The calculation can also be extended by working to higher orders in perturbation theory so that all degeneracies are lifted. It is also worthwhile to note that the advantage in using the 1D effective model lies in the drastic reduction in the degrees of freedom in certain parameter regimes. It would be interesting to also look for other quantum many-body models where this happens.

APPENDIX: 1D EFFECTIVE HAMILTONIAN

In this section, we explicitly work out the low-energy effective Hamiltonian $\tilde{H}$ for periodic boundary conditions along the legs and rungs up to second order in perturbation theory. From the Hamiltonian H_{R_i} given in Eq. (4), it is obvious that for large h, the minimum energy state is given by all up spins

$$\left|\psi_0^{(i)}\right\rangle = \otimes_{j=1}^L |0_{i,j}\rangle, \tag{A1}$$

having energy $L(\frac{1}{4} - \frac{h}{2J_\perp}) - E_g$. The next higher energy states at large h are given by one spin flip; since this can occur at any of the L rung sites, there are L such states. Since the Hamiltonian H_{R_i} is translationally invariant, we can switch to momentum basis via

$$|q\rangle = \frac{1}{\sqrt{L}} \sum_{j=1}^L e^{2iqj\pi/L} \sigma_{i,j}^x \left|\psi_0^{(i)}\right\rangle, \tag{A2}$$

where $q = 0, 1, 2, \ldots, L-1$. These states are energy eigenstates for all values of h:

$$H_{R_i}|q\rangle = \left[\cos\left(\frac{2\pi q}{L}\right) + L\left(\frac{1}{4} - \frac{h}{2J_\perp}\right) + \frac{h}{J_\perp} - 1 - E_g\right]|q\rangle. \tag{A3}$$

For even $L(> 2)$, the minimum energy eigenstate corresponds to $q = L/2$, with energy eigenvalue $L(\frac{1}{4} - \frac{h}{2J_\perp}) + \frac{h}{J_\perp} - 2 - E_g$. This state becomes degenerate with the minimum energy state at

$$h' = 2J_\perp, \tag{A4}$$

while the state itself is given by

$$\left|\psi_1^{(i)}\right\rangle = |q = L/2\rangle = \frac{1}{\sqrt{L}} \sum_{j=1}^L (-1)^j |j\rangle. \tag{A5}$$

For $L = 2$, periodic and open boundary conditions are equivalent, and $h' = J_\perp$, while $\left|\psi_0^{(i)}\right\rangle$ and $\left|\psi_1^{(i)}\right\rangle$ given by Eqs. (A1) and (A5) respectively. For odd L, the minimum energy states in this sector correspond to $(L \pm 1)/2$. This leads to a three-fold degeneracy of ground states of the rung at $h = h'$, which is beyond the scope of our consideration in this paper. We must comment here that while it is reasonable to expect that the first excited state at large h becomes degenerate with the minimum energy state as we dial down h, it is not guaranteed to be. However, our numerical investigation verifies this expectation to be correct.

1. First-order calculation

Since the first-order effective Hamiltonian is guaranteed to be at most nearest-neighbor in the effective spins, the most general form of z-rotationally invariant $\tilde{H}$ [$= J_\perp^{-1}\tilde{H}^{(1)}$; see Eq. (23)] is a nearest-neighbor XXZ model [30] in a magnetic field, given by

$$\tilde{H} = \sum_{i=1}^N \left[\tilde{J}_{xy}^{(1)}(\tau_i^x \tau_{i+1}^x + \tau_i^y \tau_{i+1}^y) + \tilde{J}_{zz}^{(1)} \tau_i^z \tau_{i+1}^z\right]$$
$$+ \tilde{h}^{(1)} \sum_{i=1}^N \tau_i^z + N\tilde{C}, \tag{A6}$$

where $N\tilde{C}$ is an irrelevant additive constant. To determine the coefficients $\tilde{J}_{xy}^{(1)}$, $\tilde{J}_{zz}^{(1)}$, and $\tilde{h}^{(1)}$ as functions of the couplings $J_\parallel/J_\perp$, $J_d^{1,2}/J_\perp$, and $\Delta h/J_\perp$ in the perturbation Hamiltonian H', we match the matrix elements of H and $\tilde{H}$ [$= J_\perp^{-1}\tilde{H}^{(1)}$; see Eq. (23)] in the following states:

$$|\Psi_0\rangle = \otimes_{i=1}^N \left|\psi_0^{(i)}\right\rangle,$$
$$|\Psi_j\rangle = \left|\psi_1^{(j)}\right\rangle \otimes_{\substack{i=1\\i\neq j}}^N \left|\psi_0^{(i)}\right\rangle,$$
$$|\Psi_{j,j+1}\rangle = \left|\psi_1^{(j)}\right\rangle \otimes \left|\psi_1^{(j+1)}\right\rangle \otimes_{\substack{i=1\\i\neq j,j+1}}^N \left|\psi_0^{(i)}\right\rangle, \tag{A7}$$

and obtain

$$\tilde{J}_{xy}^{(1)} = \frac{1}{4}\left(\frac{J_\parallel}{J_\perp} - \frac{J_d^1}{J_\perp} - \frac{J_d^2}{J_\perp}\right),$$
$$\tilde{J}_{zz}^{(1)} = \frac{1}{4L}\left(\frac{J_\parallel}{J_\perp} + \frac{J_d^1}{J_\perp} + \frac{J_d^2}{J_\perp}\right),$$
$$\tilde{h}^{(1)} = \frac{1}{2}\left[\frac{(L-1)}{L}\left(\frac{J_\parallel}{J_\perp} + \frac{J_d^1}{J_\perp} + \frac{J_d^2}{J_\perp}\right) - \frac{\Delta h}{J_\perp}\right], \tag{A8}$$

in the cases of $L > 2$. For $L = 2$ [20,25,26,29] where OBC along the rungs is equivalent to PBC, we separately work out the effective couplings as

$$\tilde{J}_{xy}^{(1)} = \frac{1}{8}\left[2\left(\frac{J_\parallel}{J_\perp}\right) - \frac{J_d^1}{J_\perp} - \frac{J_d^2}{J_\perp}\right],$$
$$\tilde{J}_{zz}^{(1)} = \frac{1}{16}\left[2\left(\frac{J_\parallel}{J_\perp}\right) + \frac{J_d^1}{J_\perp} + \frac{J_d^2}{J_\perp}\right],$$
$$\tilde{h}^{(1)} = \frac{1}{8}\left[2\left(\frac{J_\parallel}{J_\perp}\right) + \frac{J_d^1}{J_\perp} + \frac{J_d^2}{J_\perp} - 4\left(\frac{\Delta h}{J_\perp}\right)\right]. \tag{A9}$$

Similar mapping and analysis can also be done when the legs obey open boundary condition (OBC). In this case, the effective 1D model is given by $\tilde{H} + \tilde{h}'^{(1)}(\tau_1^z + \tau_N^z)$, with $\tilde{H}$ as in Eq. (A6) and its effective couplings given in Eq. (A8), where the edge inhomogeneity in the field strength, for $L > 2$, is

$$\tilde{h}'^{(1)} = -\frac{(L-1)}{4L}\left(\frac{J_\parallel}{J_\perp} + \frac{J_d^1}{J_\perp} + \frac{J_d^2}{J_\perp}\right), \tag{A10}$$

while for $L = 2$, it is

$$\tilde{h}'^{(1)} = -\frac{1}{16}\left[2\left(\frac{J_\parallel}{J_\perp}\right) + \frac{J_d^1}{J_\perp} + \frac{J_d^2}{J_\perp}\right]. \tag{A11}$$

2. Second-order calculation

We now derive the effective Hamiltonian up to the second order in perturbation theory for arbitrary rung size L and for PBC along both rungs and legs, given by $\tilde{H} = J_\perp^{-1}\tilde{H}^{(1)} + J_\perp^{-2}\tilde{H}^{(2)}$ [see Eq. (23)]. Note that $J_\perp^{-1}\tilde{H}^{(1)}$ alone has

already been derived in Appendix A 1. Note also that $\tilde{H}$ now can involve at most next-nearest-neighbor terms in effective spins. The most general z-rotationally invariant form of $\tilde{H}$ is given by

$$
\tilde{H} = \sum_{i=1}^{N} \left[\tilde{J}_{xy} \left(\tau_i^x \tau_{i+1}^x + \tau_i^y \tau_{i+1}^y \right) + \tilde{J}_{zz} \tau_i^z \tau_{i+1}^z \right] + \sum_{i=1}^{N} \left[\tilde{J}_{xy}' \left(\tau_{i-1}^x \tau_{i+1}^x + \tau_{i-1}^y \tau_{i+1}^y \right) + \tilde{J}_{zz}' \tau_{i-1}^z \tau_{i+1}^z \right]
$$

$$
+ \tilde{J}_{xyz} \sum_{i=1}^{N} \left[\tau_{i-1}^z \left(\tau_i^x \tau_{i+1}^x + \tau_i^y \tau_{i+1}^y \right) + \left(\tau_{i-1}^x \tau_i^x + \tau_{i-1}^y \tau_i^y \right) \tau_{i+1}^z \right] + \tilde{J}_{xyz}' \sum_{i=1}^{N} \left(\tau_{i-1}^x \tau_{i+1}^x + \tau_{i-1}^y \tau_{i+1}^y \right) \tau_i^z
$$

$$
+ \tilde{J}_{zzz} \sum_{i=1}^{N} \tau_{i-1}^z \tau_i^z \tau_{i+1}^z + \tilde{h} \sum_{i=1}^{N} \tau_i^z + N\tilde{C}, \tag{A12}
$$

where $N\tilde{C}$ is a constant that we ignore. Clearly, the nearest-neighbor and single-site terms in effective spins have both first- and second-order contributions (see Sec. 1 of this Appendix for the first-order contributions alone). We first consider the case of even values of L, with $L \geqslant 4$. Taking PBC along both legs and rungs, and following the same line of calculation as in Sec. 1 of this Appendix, we match the matrix elements of H and $\tilde{H}$ in the following states:

$$
|\Psi_0\rangle = \otimes_{i=1}^{N} |\psi_0^{(i)}\rangle,
$$

$$
|\Psi_j\rangle = |\psi_1^{(j)}\rangle \otimes_{\substack{i=1 \\ i \neq j}}^{N} |\psi_0^{(i)}\rangle,
$$

$$
|\Psi_{j,j+1}\rangle = |\psi_1^{(j)}\rangle \otimes |\psi_1^{(j+1)}\rangle \otimes_{\substack{i=1 \\ i \neq j,j+1}}^{N} |\psi_0^{(i)}\rangle,
$$

$$
|\Psi_{j,j+2}\rangle = |\psi_1^{(j)}\rangle \otimes |\psi_1^{(j+2)}\rangle \otimes_{\substack{i=1 \\ i \neq j,j+2}}^{N} |\psi_0^{(i)}\rangle,
$$

$$
|\Psi_{j,j+1,j+2}\rangle = |\psi_1^{(j)}\rangle \otimes |\psi_1^{(j+1)}\rangle \otimes |\psi_1^{(j+2)}\rangle \otimes_{\substack{i=1 \\ i \neq j,j+1,j+2}}^{N} |\psi_0^{(i)}\rangle. \tag{A13}
$$

We point out here that unlike the first-order perturbation theory, in the present case, application of the perturbation term $J_{\perp}^{-1} H'$ on the state of a rung in its ground-state manifold can give rise to excited states, which, in turn, involves calculation of the energy of the excited rung states. We achieve this via thermodynamic Bethe ansatz [31], and subsequently obtain

$$
\tilde{J}_{xy} = \frac{1}{4} \left(\frac{J_{||} - J_d^{\text{sum}}}{J_{\perp}} \right),
$$

$$
\tilde{J}_{zz} = \frac{1}{4} \left[\frac{1}{L} \left(\frac{J_{||} + J_d^{\text{sum}}}{J_{\perp}} \right) + \frac{F}{2} \left(\frac{J_{||} - J_d^{\text{sum}}}{J_{\perp}} \right)^2 + G \right],
$$

$$
\tilde{J}_{xy}' = \frac{F}{16} \left(\frac{J_{||} - J_d^{\text{sum}}}{J_{\perp}} \right)^2,
$$

$$
\tilde{J}_{xyz}' = -\frac{F}{16} \left(\frac{J_{||} - J_d^{\text{sum}}}{J_{\perp}} \right)^2,
$$

$$
\tilde{h} = \frac{1}{2} \left[\frac{L-1}{L} \left(\frac{J_{||} + J_d^{\text{sum}}}{J_{\perp}} \right) - \frac{\Delta h}{J_{\perp}} - \frac{F}{2} \left(\frac{J_{||} - J_d^{\text{sum}}}{J_{\perp}} \right)^2 - G \right], \tag{A14}
$$

while $\tilde{J}_{zz}'$, $\tilde{J}_{xyz}$, $\tilde{J}_{zzz}$ vanish, and the factors F and G are given by

$$
F = -2J_{\perp}^{-1} L^{-2} \sum_{m=0}^{L/2-1} \left[(1 + \cos a_m) \sum_{\substack{l_1,l_2 \\ l_2 > l_1}} \cos^2 \left(a_m f_{l_1,l_2} \right) \right]^{-1} \sum_{\substack{l_1,l_2=1 \\ l_2 > l_1}}^{L} \sum_{\substack{l_1',l_2'=1 \\ l_2' > l_1'}}^{L} \left[(-1)^\ell \cos \left(a_m f_{l_1,l_2} \right) \cos \left(a_m f_{l_1',l_2'} \right) \right],
$$

$$
G = -J_{\perp}^{-3} L^{-4} \sum_{\substack{m_1,m_2=0 \\ m_2 \neq m_1 \neq L/2}}^{L-1} X_{m_1,m_2} \sum_{j,j'=1}^{L} \frac{\exp \left[2\pi \mathrm{i}(m_1 + m_2)(j' - j)/L \right]}{\cos b_{m_1} + \cos b_{m_2} + 2}, \tag{A15}
$$

where

$$
X_{m_1,m_2} = (J_{||})^2 + \left(J_d^1 \right)^2 + \left(J_d^2 \right)^2 - 2J_{||} \left(J_d^1 \cos b_{m_2} + J_d^2 \cos b_{m_1} \right) + 2J_d^1 J_d^2 \cos \left(b_{m_2} - b_{m_1} \right), \tag{A16}
$$

and $\ell = l_1 + l_2 + l'_1 + l'_2$, $a_\alpha = 4\pi\alpha/(L-1)$, $b_\alpha = 2\pi\alpha/L$, $f_{\alpha,\beta} = \alpha - \beta + 1/2$, and h' is the strength of the magnetic field at which the rung ground states are doubly degenerate. Finally we combine the terms corresponding to $\tilde{J}'_{xy}$ and $\tilde{J}'_{xyz}$, and write the form of $\tilde{H}$ as

$$\tilde{H} = \sum_{i=1}^{N} \left[\tilde{J}_{xy}^{(2)} \left(\tau_i^x \tau_{i+1}^x + \tau_i^y \tau_{i+1}^y \right) + \tilde{J}_{zz}^{(2)} \tau_i^z \tau_{i+1}^z \right]$$
$$+ \tilde{K}_{xyz}^{(2)} \sum_{i=1}^{N} \left(\tau_{i-1}^x \tau_{i+1}^x + \tau_{i-1}^y \tau_{i+1}^y \right) \left(I_i - \tau_i^z \right) + \tilde{h}^{(2)} \sum_{i=1}^{N} \tau_i^z, \tag{A17}$$

where we define $\tilde{K}_{xyz} = \tilde{J}'_{xy} = -\tilde{J}'_{xyz}$.

Similar to the case of first-order perturbation theory, we work out the details of the effective couplings separately for $L = 2$, and get

$$\tilde{J}_{xy} = \frac{1}{8}\left(\frac{2J_{||} - J_d^{\text{sum}}}{J_\perp} \right) - \frac{1}{32J_\perp}\left(\frac{J_d^1 - J_d^2}{J_\perp} \right)^2,$$

$$\tilde{J}_{zz} = \frac{1}{16}\left(\frac{2J_{||} + J_d^{\text{sum}}}{J_\perp} \right) + \frac{1}{32J_\perp}\left(\frac{J_d^1 - J_d^2}{J_\perp} \right)^2$$
$$- \frac{3}{128J_\perp}\left(\frac{2J_{||} - J_d^{\text{sum}}}{J_\perp} \right)^2,$$

$$\tilde{J}'_{xy} = \frac{1}{64J_\perp}\left(\frac{J_d^1 - J_d^2}{J_\perp} \right)^2 - \frac{1}{128J_\perp}\left(\frac{2J_{||} - J_d^{\text{sum}}}{J_\perp} \right)^2,$$

$$\tilde{J}'_{zz} = \frac{1}{64J_\perp}\left(\frac{J_d^1 - J_d^2}{J_\perp} \right)^2,$$

$$\tilde{J}_{xyz} = \frac{1}{64J_\perp}\left(\frac{J_d^1 - J_d^2}{J_\perp} \right)^2,$$

$$\tilde{J}'_{xyz} = \frac{1}{64J_\perp}\left(\frac{J_d^1 - J_d^2}{J_\perp} \right)^2 + \frac{1}{128J_\perp}\left(\frac{2J_{||} - J_d^{\text{sum}}}{J_\perp} \right)^2,$$

$$\tilde{J}_{zzz} = -\frac{1}{64J_\perp}\left(\frac{J_d^1 - J_d^2}{J_\perp} \right)^2,$$

$$\tilde{h}^{(1)} = \frac{1}{8}\left(\frac{2J_{||} + J_d^{\text{sum}}}{J_\perp} \right) - \frac{\Delta h}{2} + \frac{1}{64J_\perp}\left(\frac{J_d^1 - J_d^2}{J_\perp} \right)^2$$
$$+ \frac{3}{64J_\perp}\left(\frac{2J_{||} - J_d^{\text{sum}}}{J_\perp} \right)^2. \tag{A18}$$

Unlike the case of $L \geqslant 4$, in this case, all effective coupling constants are nonvanishing, and the effective Hamiltonian is given by Eq. (A12). Note that for $J_d^{1,2} = 0$ as well as $J_d^1 = J_d^2 \neq 0$, the 1D effective Hamiltonian for $L = 2$ also takes the form given by Eq. (A17), while the corresponding coupling constants for $L = 2$ are given by Eqs. (A14) only when $J_d^{1,2} = 0$.

3. Open rungs: Outlines

Here we present the details required to work out the 1D effective Hamiltonian when open boundary condition (OBC) along the rungs is considered. In this case, exact calculation of the degenerate ground states and the strength of the magnetic field at which the degeneracy occurs is difficult for arbitrary L. However, our numerical analysis suggests that for open (periodic) boundary condition along the rungs (legs), and for arbitrary L, $|\psi_0^{(i)}\rangle$ is still given by Eq. (A1), while $|\psi_1^{(i)}\rangle$ is found in the $\langle Z_i \rangle = L - 2$ sector and has the form

$$\left| \psi_1^{(i)} \right\rangle = \sum_{j=1}^{L} a_j |j\rangle, \tag{A19}$$

with $a_j \in \mathbb{R}$, and $\sum_{j=1}^{L} a_j^2 = 1$. Note further that due to Z_2 symmetry, $a_1 = \pm a_L$. The system parameters of the effective Hamiltonian depends on the coefficients $\{a_j, j = 1, \ldots, L\}$. For example, the first-order effective Hamiltonian for the case of OBC (PBC) along the rungs (legs) with $L \geqslant 3$ would still be given by Eq. (A6), with

$$\tilde{J}_{xy}^{(1)} = \frac{1}{4}\left[\frac{J_{||}}{J_\perp} + A_0\left(\frac{J_d^1}{J_\perp} + \frac{J_d^2}{J_\perp} \right) \right],$$

$$\tilde{J}_{zz}^{(1)} = \frac{1}{16}\left[(4 - L + A_1)\frac{J_{||}}{J_\perp} \right.$$
$$\left. + (L - 1 + A_3 - 2A_2)\left(\frac{J_d^1}{J_\perp} + \frac{J_d^2}{J_\perp} \right) \right],$$

$$\tilde{h}^{(1)} = \frac{1}{8}\left[(L - A_1)\frac{J_{||}}{J_\perp} + (L - 1 - A_3)\left(\frac{J_d^1}{J_\perp} + \frac{J_d^2}{J_\perp} \right) - 4\frac{\Delta h}{J_\perp} \right], \tag{A20}$$

where A_i, $i = 0, 1, 2, 3$, are constants given by

$$A_0 = \sum_{j=1}^{L-1} a_j a_{j+1}, \tag{A21}$$

$$A_1 = L \sum_{j=1}^{L} a_j^4 + (2L - 8) \sum_{j=1}^{L} \sum_{k<j} a_j^2 a_k^2, \tag{A22}$$

$$A_2 = L - 3 + 2a_1^2, \tag{A23}$$

$$A_3 = (L-1)\left\{ \sum_{j=1}^{L-1} a_j^2 a_{j+1}^2 + a_L^2 a_1^2 \right\}$$
$$+ (L-3)\left\{ \sum_{j=1}^{L-1} a_j^2 a_1^2 + \sum_{j=2}^{L} a_L^2 a_j^2 \right\}$$
$$+ (L-5)\left\{ \sum_{j=1}^{L-1} \sum_{k=j+2}^{L} a_j^2 a_k^2 + \sum_{j=2}^{L} \sum_{k=j}^{L-1} a_k^2 a_j^2 \right\}. \tag{A24}$$

[1] M. A. Nielsen and I. L. Chuang, *Quantum Computation and Quantum Information* (Cambridge University Press, Cambridge, 2010); M. M. Wilde, *Quantum Information Theory*, 2nd ed. (Cambridge University Press, Cambridge, 2017).

[2] I. Bose, Low-dimensional quantum spin systems, in *Field Theories in Condensed Matter Physics* (Hindustan Book Agency, Gurgaon, 2001), pp. 359–408; A. Vasiliev, O. Volkova, E. Zvereva, and M. Markina, npj Quantum Mater. **3**, 18 (2018).

[3] L. Amico, R. Fazio, A. Osterloh, and V. Vedral, Rev. Mod. Phys. **80**, 517 (2008); J. I. Latorre and A. Riera, J. Phys. A: Math. Theor. **42**, 504002 (2009).

[4] N. Laflorencie, Phys. Rep. **646**, 1 (2016); G. D. Chiara and A. Sanpera, Rep. Prog. Phys. **81**, 074002 (2018).

[5] K. Modi, A. Brodutch, H. Cable, T. Paterek, and V. Vedral, Rev. Mod. Phys. **84**, 1655 (2012); A. Bera, T. Das, D. Sadhukhan, S. S. Roy, A. Sen(De), and U. Sen, Rep. Prog. Phys. **81**, 024001 (2018).

[6] S. Bose, Phys. Rev. Lett. **91**, 207901 (2003); S. Bose, A. Bayat, P. Sodano, L. Banchi, and P. Verrucchi, in *Quantum State Transfer and Network Engineering*, edited by G. M. Nikolopoulos and I. Jex (Springer, Berlin, 2013), pp. 1–38.

[7] R. Raussendorf and H. J. Briegel, Phys. Rev. Lett. **86**, 5188 (2001); R. Raussendorf, D. E. Browne, and H. J. Briegel, Phys. Rev. A **68**, 022312 (2003); H. J. Briegel, D. E. Browne, W. Dür, R. Raussendorf, and M. Van den Nest, Nat. Phys. **5**, 19 (2009); T.-C. Wei, Adv. Phys.: X **3**, 1461026 (2018).

[8] E. Dennis, A. Kitaev, A. Landahl, and J. Preskill, J. Math. Phys. **43**, 4452 (2002); A. Kitaev, Ann. Phys. **321**, 2 (2006); H. Bombin and M. A. Martin-Delgado, Phys. Rev. Lett. **97**, 180501 (2006); **98**, 160502 (2007).

[9] R. Horodecki, P. Horodecki, M. Horodecki, and K. Horodecki, Rev. Mod. Phys. **81**, 865 (2009); O. Gühne and G. Tóth, Phys. Rep. **474**, 1 (2009).

[10] U. Schollwöck, Rev. Mod. Phys. **77**, 259 (2005); F. Verstraete, V. Murg, and J. Cirac, Adv. Phys. **57**, 143 (2008); U. Schollwöck, Ann. Phys. **326**, 96 (2011); R. Orús, *ibid.* **349**, 117 (2014); J. C. Bridgeman and C. T. Chubb, J. Phys. A: Math. Theor. **50**, 223001 (2017).

[11] F. Verstraete and J. I. Cirac, arXiv:cond-mat/0407066; G. Vidal, Phys. Rev. Lett. **99**, 220405 (2007); **101**, 110501 (2008); M. Rizzi, S. Montangero, and G. Vidal, Phys. Rev. A **77**, 052328 (2008); M. Aguado and G. Vidal, Phys. Rev. Lett. **100**, 070404 (2008); L. Cincio, J. Dziarmaga, and M. M. Rams, *ibid.* **100**, 240603 (2008); G. Evenbly and G. Vidal, Phys. Rev. B **79**, 144108 (2009).

[12] D. Porras and J. I. Cirac, Phys. Rev. Lett. **92**, 207901 (2004); D. Leibfried, E. Knill, S. Seidelin, J. Britton, R. B. Blakestad, J. Chiaverini, D. B. Hume, W. M. Itano, J. D. Jost, C. Langer *et al.*, Nature (London) **438**, 639 (2005); T. Monz, P. Schindler, J. T. Barreiro, M. Chwalla, D. Nigg, W. A. Coish, M. Harlander, W. Hänsel, M. Hennrich, and R. Blatt, Phys. Rev. Lett. **106**, 130506 (2011); S. Korenblit, D. Kafri, W. C. Campbell, R. Islam, E. E. Edwards, Z.-X. Gong, G.-D. Lin, L.-M. Duan, J. Kim, K. Kim, and C. Monroe, New J. Phys. **14**, 095024 (2012); J. G. Bohnet, B. C. Sawyer, J. W. Britton, M. L. Wall, A. M. Rey, M. Foss-Feig, and J. J. Bollinger, Science **352**, 1297 (2016).

[13] R. Barends, J. Kelly, A. Megrant, A. Veitia, D. Sank, E. Jeffrey, T. C. White, J. Mutus, A. G. Fowler, B. Campbell *et al.*, Nature (London) **508**, 500 (2014); Y. Yanay, J. Braumüller, S. Gustavsson, W. D. Oliver, and C. Tahan, npj Quantum Inf. **6**, 58 (2020).

[14] L. M. K. Vandersypen and I. L. Chuang, Rev. Mod. Phys. **76**, 1037 (2005); C. Negrevergne, T. S. Mahesh, C. A. Ryan, M.

Ditty, F. Cyr-Racine, W. Power, N. Boulant, T. Havel, D. G. Cory, and R. Laflamme, Phys. Rev. Lett. **96**, 170501 (2006).

[15] M. Schechter and P. C. E. Stamp, Phys. Rev. B **78**, 054438 (2008); C. E. Bradley, J. Randall, M. H. Abobeih, R. C. Berrevoets, M. J. Degen, M. A. Bakker, M. Markham, D. J. Twitchen, and T. H. Taminiau, Phys. Rev. X **9**, 031045 (2019).

[16] M. Greiner, O. Mandel, T. Esslinger, T. W. Hänsch, and I. Bloch, Nature (London) **415**, 39 (2002); L.-M. Duan, E. Demler, and M. D. Lukin, Phys. Rev. Lett. **91**, 090402 (2003); I. Bloch, J. Phys. B: At., Mol. Opt. Phys. **38**, S629 (2005); I. Bloch, J. Dalibard, and W. Zwerger, Rev. Mod. Phys. **80**, 885 (2008); J. Struck, M. Weinberg, C. Ölschläger, P. Windpassinger, J. Simonet, K. Sengstock, R. Höppner, P. Hauke, A. Eckardt, M. Lewenstein, and L. Mathey, Nat. Phys. **9**, 738 (2013).

[17] W. Heisenberg, Z. Phys. **49**, 619 (1928); Y. Okwamoto, J. Phys. Soc. Jpn. **53**, 2434 (1984); S. S. Aplesnin, Phys. Solid State **41**, 103 (1999); Z. Weihong, R. H. McKenzie, and R. R. P. Singh, Phys. Rev. B **59**, 14367 (1999); B. Costa and A. Pires, J. Magn. Magn. Mater. **262**, 316 (2003); A. Cuccoli, G. Gori, R. Vaia, and P. Verrucchi, J. Appl. Phys. **99**, 08H503 (2006); H. Ju, A. B. Kallin, P. Fendley, M. B. Hastings, and R. G. Melko, Phys. Rev. B **85**, 165121 (2012); R. Verresen, F. Pollmann, and R. Moessner, *ibid.* **98**, 155102 (2018); O. S. Saríyer, Philos. Mag. **99**, 1787 (2019).

[18] A. B. Kallin, M. B. Hastings, R. G. Melko, and R. R. P. Singh, Phys. Rev. B **84**, 165134 (2011); H. F. Song, N. Laflorencie, S. Rachel, and K. Le Hur, *ibid.* **83**, 224410 (2011); L. Lima, Solid State Commun. **309**, 113836 (2020).

[19] E. Ercolessi, Mod. Phys. Lett. A **18**, 2329 (2003); N. B. Ivanov, Condens. Matter Phys. **12**, 435 (2009).

[20] E. Dagotto and T. M. Rice, Science **271**, 618 (1996); M. T. Batchelor, X.-W. Guan, A. Foerster, and H.-Q. Zhou, New J. Phys. **5**, 107 (2003); M. Batchelor, X.-W. Guan, A. Foerster, A. Tonel, and H.-Q. Zhou, Nucl. Phys. B **669**, 385 (2003).

[21] M. T. Batchelor, X. W. Guan, N. Oelkers, and Z. Tsuboi, Adv. Phys. **56**, 465 (2007).

[22] Y. Li, T. Shi, B. Chen, Z. Song, and C.-P. Sun, Phys. Rev. A **71**, 022301 (2005); G. M. Almeida, A. M. Souza, F. A. de Moura, and M. L. Lyra, Phys. Lett. A **383**, 125847 (2019).

[23] J.-L. Song, S.-J. Gu, and H.-Q. Lin, Phys. Rev. B **74**, 155119 (2006); Y. Chen, P. Zanardi, Z. D. Wang, and F. C. Zhang, New J. Phys. **8**, 97 (2006); H. S. Dhar and A. Sen(De), J. Phys. A: Math. Theor. **44**, 465302 (2011); J. Ren and S. Zhu, Int. J. Quantum Inf. **09**, 531 (2011); A. M. Läuchli and J. Schliemann, Phys. Rev. B **85**, 054403 (2012); H. S. Dhar, A. Sen(De), and U. Sen, New J. Phys. **15**, 013043 (2013); R. A. Santos, C.-M. Jian, and R. Lundgren, Phys. Rev. B **93**, 245101 (2016); S. Singha Roy, H. S. Dhar, D. Rakshit, A. Sen(De), and U. Sen, J. Magn. Magn. Mater. **444**, 227 (2017); S.-H. Li, Q.-Q. Shi, M. T. Batchelor, and H.-Q. Zhou, New J. Phys. **19**, 113027 (2017).

[24] J. Schliemann and A. M. Läuchli, J. Stat. Mech.: Theory Exp. (2012) P11021.

[25] K. Totsuka, Phys. Rev. B **57**, 3454 (1998); T. Tonegawa, T. Nishida, and M. Kaburagi, Phys. B: Condens. Matter **246–247**, 368 (1998); G. Chaboussant, M. H. Julien, Y. Fagot-Revurat, M. Hanson, L. P. Lévy, C. Berthier, M. Horvatic, and O. Piovesana, Eur. Phys. J. B **6**, 167 (1998).

[26] F. Mila, Eur. Phys. J. B **6**, 201 (1998).

[27] A. Tribedi and I. Bose, Phys. Rev. A **79**, 012331 (2009).

[28] K. Kawano and M. Takahashi, J. Phys. Soc. Jpn. **66**, 4001 (1997).

[29] K. Tandon, S. Lal, S. K. Pati, S. Ramasesha, and D. Sen, Phys. Rev. B **59**, 396 (1999).

[30] M. E. Fisher, Am. J. Phys. **32**, 343 (1964); T. Giamarchi, *Quantum Physics in One Dimension*, International Series of Monographs on Physics (Clarendon Press, Oxford, 2004); F. Mila, Eur. J. Phys. **21**, 499 (2000).

[31] F. Franchini, *An Introduction to Integrable Techniques for One-Dimensional Quantum Systems*, Lecture Notes in Physics (Springer, Cham, Switzerland, 2017).

[32] F. Mila and K. P. Schmidt, in *Introduction to Frustrated Magnetism: Materials, Experiments, Theory*, edited by C. Lacroix, P. Mendels, and F. Mila (Springer, Berlin, 2011), pp. 537–559.

[33] S. Chen, L. Wang, and Y. P. Wang, Eur. Phys. J. B **57**, 265 (2007).

[34] H.-J. Mikeska and A. K. Kolezhuk, in *Quantum Magnetism*, edited by U. Schollwöck, J. Richter, D. J. J. Farnell, and R. F. Bishop (Springer, Berlin, 2004), pp. 1–83.

[35] A. Dutta, G. Aeppli, B. K. Chakrabarti, U. Divakaran, T. F. Rosenbaum, and D. Sen, *Quantum Phase Transitions in Transverse Field Spin Models: From Statistical Physics to Quantum Information* (Cambridge University Press, Cambridge, 2015).

[36] E. Lieb, T. Schultz, and D. Mattis, Ann. Phys. **16**, 407 (1961); E. Barouch, B. M. McCoy, and M. Dresden, Phys. Rev. A **2**, 1075 (1970); E. Barouch and B. M. McCoy, *ibid.* **3**, 786 (1971); **3**, 2137 (1971).

[37] I. Titvinidze and G. I. Japaridze, Eur. Phys. J. B **32**, 383 (2003); P. Lou, W.-C. Wu, and M.-C. Chang, Phys. Rev. B **70**, 064405 (2004); M.-F. Yang, Phys. Rev. A **71**, 030302(R) (2005); T. Krokhmalskii, O. Derzhko, J. Stolze, and T. Verkholyak, Phys. Rev. B **77**, 174404 (2008); V. Derzhko, O. Derzhko, and J. Richter, *ibid.* **83**, 174428 (2011).

[38] T. J. Osborne and M. A. Nielsen, Phys. Rev. A **66**, 032110 (2002).

[39] C. H. Bennett, D. P. DiVincenzo, J. A. Smolin, and W. K. Wootters, Phys. Rev. A **54**, 3824 (1996).

[40] A. Peres, Phys. Rev. Lett. **77**, 1413 (1996); M. Horodecki, P. Horodecki, and R. Horodecki, Phys. Lett. A **223**, 1 (1996); K. Życzkowski, P. Horodecki, A. Sanpera, and M. Lewenstein, Phys. Rev. A **58**, 883 (1998); G. Vidal and R. F. Werner, *ibid.* **65**, 032314 (2002); J. Lee, M. S. Kim, Y. J. Park, and S. Lee, J. Mod. Opt. **47**, 2151 (2000); M. B. Plenio, Phys. Rev. Lett. **95**, 090503 (2005).

[41] C. B. Pushpan, H. K J, and A. K. Pal, Phys. Lett. A **511**, 129543 (2024).

[42] J. Almeida, M. A. Martin-Delgado, and G. Sierra, J. Phys. A: Math. Theor. **41**, 485301 (2008); Phys. Rev. B **77**, 094415 (2008).

[43] P. Krammer, H. Kampermann, D. Bruß, R. A. Bertlmann, L. C. Kwek, and C. Macchiavello, Phys. Rev. Lett. **103**, 100502 (2009); A. Scheie, P. Laurell, A. M. Samarakoon, B. Lake, S. E. Nagler, G. E. Granroth, S. Okamoto, G. Alvarez, and D. A. Tennant, Phys. Rev. B **103**, 224434 (2021).

[44] Quantum Information and Computation library (QIClib), Version 1.0 (2017), https://github.com/titaschanda/QIClib.